IOWA STATE UNIVERSITY
Digital Repository

2007

Nondestructive evaluation of a carbon fiber wing spar using air-coupled ultrasound

Adam Howard Kite

Iowa State University

Part of the Aerospace Engineering Commons

Nondestructive evaluation of a carbon fiber wing spar
using air-coupled ultrasound

by

Adam Howard Kite

A thesis submitted to the graduate faculty
in partial fulfillment of the requirements for the degree of
MASTER OF SCIENCE

Major: Aerospace Engineering

Program of Study Committee:
David K. Hsu, Major Professor
Vinay Dayal
Palaniappa A. Molian

Iowa State University

Ames, Iowa

2007

UMI Number: 1446040

UMI®

TABLE OF CONTENTS

LIST OF TABLES

LIST OF FIGURES

ACKNOWLEDGEMENTS

ABSTRACT

Nondestructive evaluation techniques for imaging flaws in a solid composite laminate and a method to determine the porosity content by processing micrograph images of the laminate are discussed in this thesis. Air-coupled ultrasound, the computer aided tap tester, and pitch-catch contact ultrasound are the nondestructive methods employed for the inspection of a carbon fiber reinforced composite main wing spar. Impact damage and foreign object inclusions have been inspected with all three methods. These methods have been shown to be successful in locating the test article defects. The determination of porosity levels from micrograph images is presented as a possible alternative to the acid digestion method. The image processing method developed utilizes a free open-source software package to process micrograph images of the test sample. The image processing method can be automated with simple scripts within the software package. The results from the image processing method are shown to correlate well with the acid digestion results. This research was aimed at advancing the inspection technology for an industrial composite structure. The results indicate that air-coupled ultrasound can potentially be a low cost alternative to other inspection techniques.

CHAPTER 1.   INTRODUCION

Air-coupled ultrasound has gained popularity in the past years as a noninvasive inspection procedure. The objective of this research was to evaluate the possibility of using air-coupled ultrasound for the nondestructive evaluation of industrial aerospace components. A laboratory scanning system and a portable, low cost, manual scanner were evaluated. Cirrus Design Corporation has developed a carbon composite main wing spar and expressed interest in air-coupled ultrasonic testing as a non-contact, potentially cost-effective technique for inspecting the spar(1). To assess the feasibility of applying air-coupled ultrasonic inspection to the geometry of the wing spar, Cirrus provided the Center for Nondestructive Evaluation(CNDE) at Iowa State University with fiberglass test articles that geometrically represent sections of a spar(2). These preliminary studies produced encouraging results and demonstrated that air-coupled ultrasound(UT) can be implemented with special high efficiency air-coupled transducers driven by portable flaw detectors. These interactions led to a comprehensive research project at CNDE that drew funding from Cirrus, the FAA, and the American Society of Nondestructive Testing(ASNT). The research was to investigate inspection techniques for the Cirrus carbon spar, mainly by air UT, but other methods developed at CNDE such as the Computer Aided Tap Tester(CATT) from Advanced Structural Imaging(3) and pitch-catch ultrasonics were applied as well.

Air-coupled ultrasonic testing is a non-contact, non-contaminating inspection method and is therefore attractive to industrial applications in a manufacturing environment. Compared to conventional water-coupled ultrasonic inspection using squirters, air UT has substantially lower costs. Air-coupled ultrasonic instruments have gained maturity in recent years and are available in compact portable forms. Special high efficiency transducers, such as the "Gas Matrix Piezoelectric (GMP)" transducers developed by the Ultran Group(4), have increased the capabilities of air UT for composite inspection. The daunting hurdle of extreme impedance mismatch between air and solid has been partially overcome by better transducers and more advanced electronics. In this work, both transducers from QMI, Inc.(5) containing piezoceramic disk and the Ultran GMP probes were used. Like conventional UT, the inspection with air-coupled UT is also best employed with imaging methods so as to benefit from the interpretation of a visual image by the inspector. In the laboratory, a mechanized scanner was used. For potential future implementation on the shop floor, a portable, manual, and low-cost C-scan

technique, known as the Generic Scanner(GenScan), developed under separate FAA funding, was also exploited and applied on the spar(6). The main inspection concern of the spar was impact damage. Test articles that represent the spar geometry were supplied by Cirrus. The first carbon test spar section was provided with impact damage already induced by Cirrus. Impacts were induced at CNDE on the additional spar sections provided by Cirrus. In addition to impact damage, air UT was also used in the detection and imaging of foreign objects (Grafoil and Teflon) in CFRP laminate specimens temporarily made available to CNDE.

Tests were performed to understand the microstructure of the composite carbon test articles. As a preparatory step, some cutting, polishing, and optical microscopy was performed to examine the ply lay-up, ply drop-off, laminate interfaces, and porosity levels in the material. While examining the porosity levels of the test articles supplied by Cirrus an image processing method was developed as an alternative to the often used acid digestion method. The image processing method uses a free software to process micrograph images. The micrographs are examined to obtain an area of porosity that is recorded as a percentage. The method was validated by examining laboratory samples with porosity levels known from acid digestion. The porosity levels found from image processing compared well with those results from acid digestion.

CHAPTER 2.   MATERIAL CHARACTERIZATION

2.1   Test Samples

The three main spar samples used for testing were supplied by Cirrus Design Corp. and can be seen in Fig. 2.1. These test articles were prepared by Cirrus to represent the nominal geometry of the actual spar only. The glass fiber spar(GS1) was supplied to CNDE during the exploratory study in May, 2005. The first carbon spar(CS1) was provided at the kick-off meeting on December 20, 2005. The second carbon spar(CS2) was provided undamaged to CNDE at the end of July, 2006.

Figure 2.1   The three spar samples used for examination. They are from
left to right the CS1, GS1, and CS2.

All three spars have a cross section similar to that shown in Fig. 2.2. The geometry of each of the spar samples is shown in Table 2.1. It should be noted that the ply drop-off area of CS1 and CS2 was a smooth slope that transitioned from the thick web to the thin web while GS1 had noticeable steps of thickness change in ply drop-off area.

Test Spar Geometry						
Spar	Length	Width	Depth	Cap 1	Cap 2	Thin Web
GS1	33.00	8.50	4.00	0.50	0.56	0.13
CS1	17.50	8.50	3.00	0.38	0.44	0.13
CS2	19.00	8.50	3.00	0.50	0.56	0.13

Table 2.1   The length, width, depth, and thickness of both caps and the thin web listed in inches for the three spar samples.

2.2   Microscopic Examination

It was desired to find out more about the lay-up and the general porosity content of the test samples as both affect the propagation of the ultrasonic wave. Nonuniform porosity content can affect the imaging process even when no specific flaw is present. To learn more about the microstructure, small samples were cut from the five major regions of the spar. The five regions under inspection are the cap, radius, thick web, thin web, and ply drop-off. The five regions are labeled in Fig. 2.2. The small samples taken from each region were mounted in epoxy resin pucks and polished to make the fibers visible under the microscope.
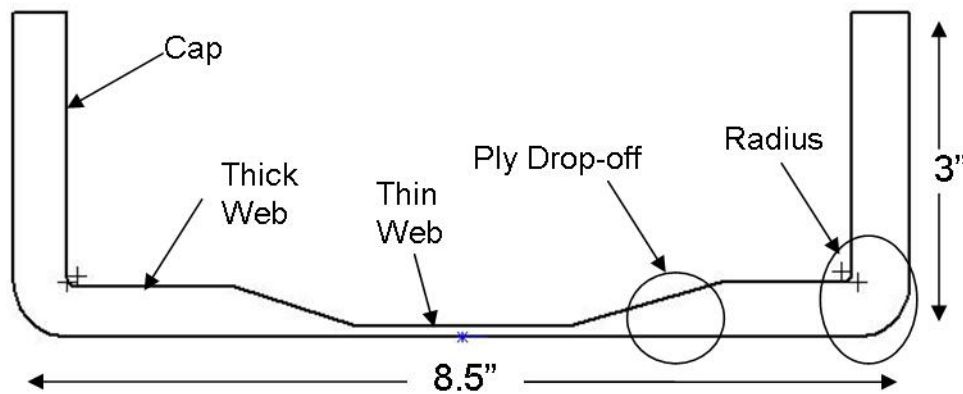
Figure 2.2   The five major areas of microscopic inspection.

2.2.1 Lay-up

The polished pucks were examined using a Nikon Epiphot 200 inverted stage microscope. Sequential micrographs were taken across the lay-up to "stitch" together composite photos of the cross sectional view of the different regions. The purpose of the micrographs was to get a general idea of fiber orientation. The fiber orientation is revealed by looking at the microscopic image where the 0° fibers appear circular while the 45° fibers show up as ovals. The 90° fibers appear as long strands or cylinders. With this method it is impossible to tell if the 45° fibers are in the plus or minus direction. The appearance of each type of fiber is shown in Fig. 2.3. A sample of an assembled composite image can be seen in Fig. 2.4.

0° Fibers   90° Fibers   ±45° Fibers   ~175 μm
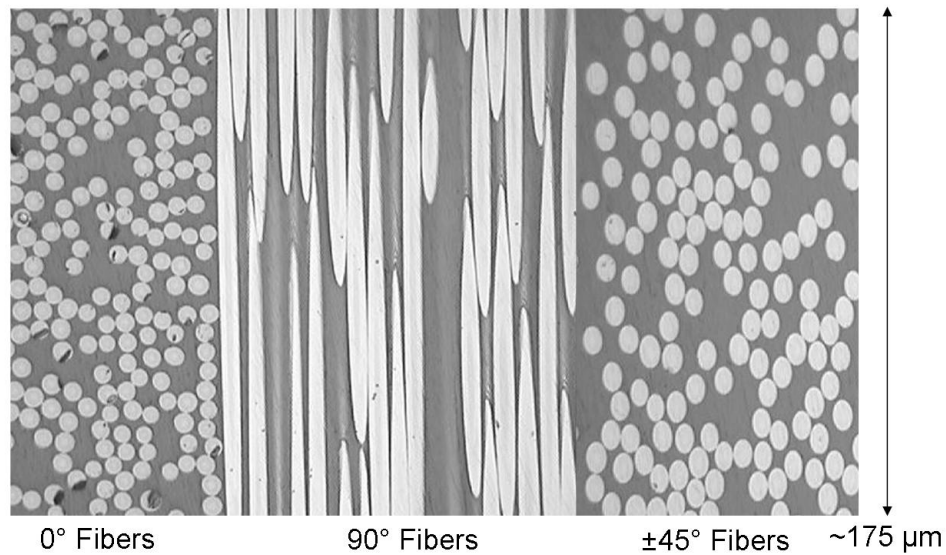
Figure 2.3   Fiber direction identification from micrograph image. The average fiber diameter is 7 μm.

←→| ~105 μm   0°fibers   45°fibers   90°fibers
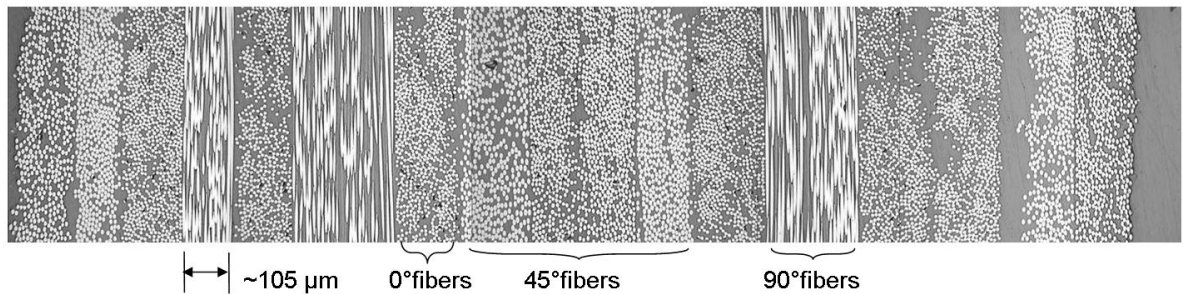
Figure 2.4   A micrograph showing different layers of fiber orientation.

2.2.2 Porosity

Micrographs were taken from each of the five areas at 50x magnification. The porosity was readily visible as dark black regions while viewing a large area of the sample. These images provided a very rough estimate of the amount of porosity present in the test samples. The porosity levels present in the test articles do not represent the characteristics of the production spars in any way. A representative micrograph from each area can be seen in Fig. 2.5. During the porosity investigation an image processing method was developed to estimate the porosity levels present in the test samples. This method analyzes micrograph images of the test sample and is presented in more detail in the following chapter.

CS1

| Cap | Radius | Thick Web | Thin Web | Ply Drop-off |

CS2

| Cap | Radius | Thick Web | Thin Web | Ply Drop-off |

GS1

| Cap | Radius | Thick Web | Thin Web | Ply Drop-off |
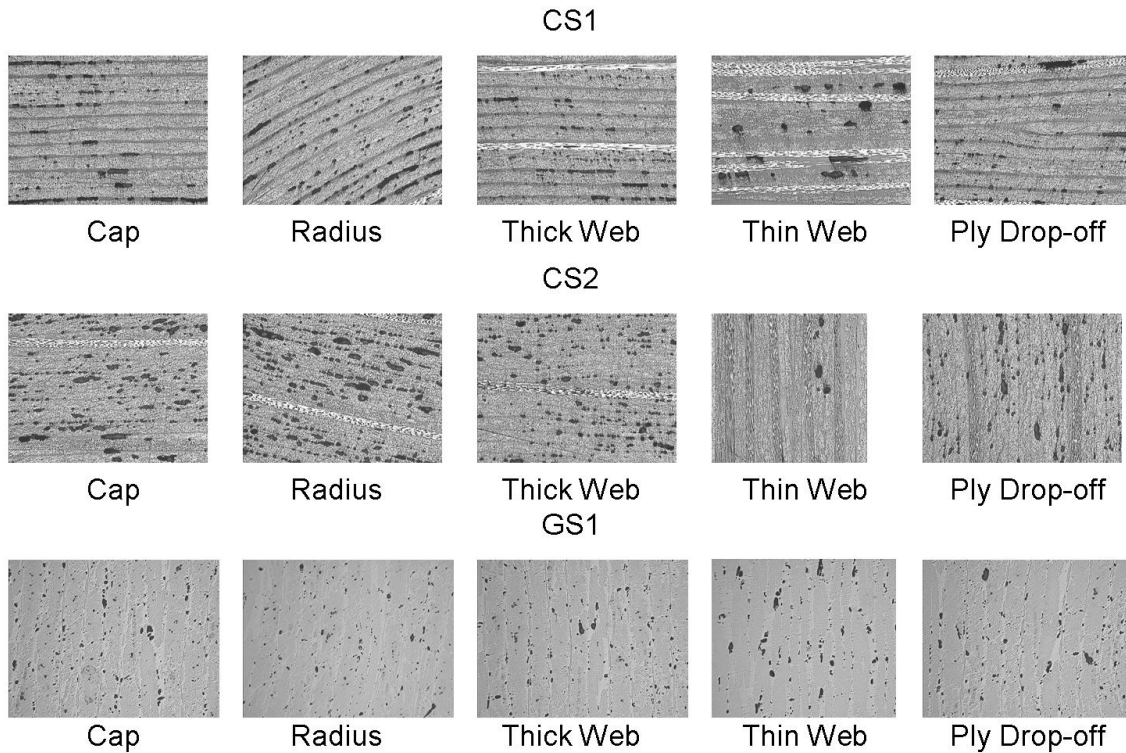
Figure 2.5   Porosity images from each area of the three spar sections.

CHAPTER 3. IMAGE PROCESSING

Image processing can be used to determine the level of porosity present in micrographs of a composite sample. Image processing requires only micrographs of a polished sample and a software package to process the micrographs. This method does not require the use of any harmful acids or other special equipment and may be used as an alternative to the traditional methods. Image processing has been used by Daniel(7) to establish a correlation of the ultrasonic attenuation in a material with porosity content and by Hsu(8) to obtain statistical data on the size, shape, and orientation of pores. The technique described in this paper has been shown to work on both graphite-epoxy and glass-epoxy composites. Porosity can arise from improper manufacturing process controls such as incorrect vacuum pressure, inadequate resin bleed off, loss of cure pressure, and improper cure temperatures. Porosity may also be caused by material factors like out dated prepregs or elevated absorbed moisture levels in the uncured composite material. The porosity content of a composite structure is critical to the overall strength and performance of the structure. For this reason it is often necessary to quantify the amount of porosity present in components for certain applications. The quantification of porosity content can be done by both nondestructive and destructive methods. Nondestructive methods include ultrasonic attenuation(9), infrared thermography(10), and X-ray. Matrix removal by acid digestion and burn-off are the most prevalent destructive methods utilized to determine porosity content(11).

3.1 Experimental Methods

3.1.1 Samples

Six groups of samples were examined in this study. The first four groups are laboratory prepared samples containing varying amounts of porosity. These were analyzed by both the image processing technique described here and the acid digestion technique to evaluate the effectiveness of the image processing method. The preparation of the samples and the acid digestion experiments were performed by laboratories outside of CNDE. Ultrasound was used to classify the uniformity of the distribution of the porosity in the laboratory samples. The remaining two groups were samples taken from actual production components of an aerospace structure. Samples A1-A6 are 16 ply unidirectional carbon/epoxy laminates containing varying

levels of porosity between 0.1 and 6.5 percent voids by volume as determined by acid digestion. Samples B1-B6 are 16 ply quasi-isotropic carbon/epoxy laminates with a [45/0/90]2S lay-up containing porosity levels between 0.34 and 5.33 percent voids by volume. Samples D1-D6 are 8 ply carbon/epoxy laminates of woven prepregs with a coarse weave pattern that contain porosity levels between 0.01 and 5.09 percent voids by volume. Samples G1-G9 are laminates of the carbon/PMR-15 system with woven plies containing 2.51-11.9 percent voids by volume and are known to have very uniform porosity levels throughout. The acid digestion results represent an average value obtained from four different regions on the test sample and the results from each specimen can be seen in Table 3.1. The sample groups from the production components are designated E1-E10 and F1-F5. The E group samples were removed from a carbon/epoxy component ranging in thickness from 0.125 to 0.5 inches. The F group samples are glass/epoxy with a thickness range of 0.125 to 0.5 inch.

Porosity levels from acid digestion								
Group	1	2	3	4	5	6	7	8	9
A	6.51	2.04	1.89	1.14	0.10	6.51	—	—	—
B	4.05	2.82	3.87	1.25	0.34	5.33	—	—	—
C	5.09	1.58	3.41	1.65	0.01	5.33	—	—	—
D	2.51	4.21	4.17	6.05	8.82	9.13	9.69	11.90	11.50

Table 3.1   The porosity levels obtained from the acid digestion method for the sample groups.

3.1.2   Microscopy

The composite samples were mounted using the Epoxicure metallurgical mounting system. The mounted samples were polished through 0.3 micron abrasives. The polished mounts were then placed on an inverted stage microscope where digital micrographs were captured at a magnification of 50X. At this magnification both the porosity and a large sample area were readily visible.

3.1.3   Image Analysis

The purpose of image processing is to eliminate the fiber and resin rich areas (shown in Fig. 3.1) from the image while leaving the porosity. This elimination is done by thresholding and filtering. Thresholding creates a binary image by turning every pixel with a value above the threshold white, and below, black. The filter's smoothing action creates a grayscale image from the binary image. Erosion occurs in both the porosity and the small dark areas remaining in the fiber and resin rich area. By repeating the thresholding and filtering process, the non-porosity dark areas in the fiber and resin rich areas are removed. The number of iterations to
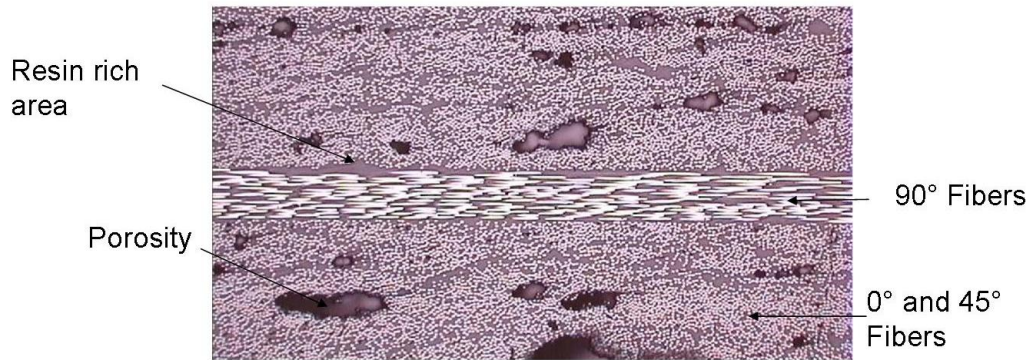
Figure 3.1   Sample micrograph showing key features of the typical micrograph image for processing. This image is of an area approximately 2.56 mm wide by 1.92 mm tall.

be used is determined during the manual thresholding phase and is dependent on the initial contrast between the porosity and the remaining area of the micrograph. It was found that fewer iterations were needed to eliminate the fibers and resin rich areas from the images with greater initial contrast. It is important that all the micrographs of a sample set be taken at the same time with the same lighting conditions to produce consistent images if the automated process is to be used. The typical micrograph shown in this thesis represents an area of 2.56 mm wide by 1.92 mm tall. ImageTool, the open-source software from UTHSCSA(12) was used to process the images from their original state to a binary version where black and white pixels could be counted to obtain an area of porosity measurement. The processing can be done manually or simple scripts can be written within the ImageTool software to automate the process. A sample of the script used can be found in the Appendix. To determine the threshold values to use for the automated process, five images were manually thresholded to remove the fibers and resin rich areas. The threshold values were then averaged to obtain the values to be used. The process for obtaining the threshold values is described next and the micrograph images as seen by the operator are shown in Fig. 3.2. The manual threshold values are obtained by opening the original image in ImageTool. The original image (Fig. 3.2a) may be in color or grayscale, but a color image must be converted to grayscale by using the *color-to-grayscale* command under the processing menu. Next, the *manual threshold* option is selected from the processing menu. This option will overlay the image with red pixels and produce a slide bar in a window with values ranging from 0-255. The red pixels represent the area that would be set as black if the image was thresholded at the current settings on the slide bar.
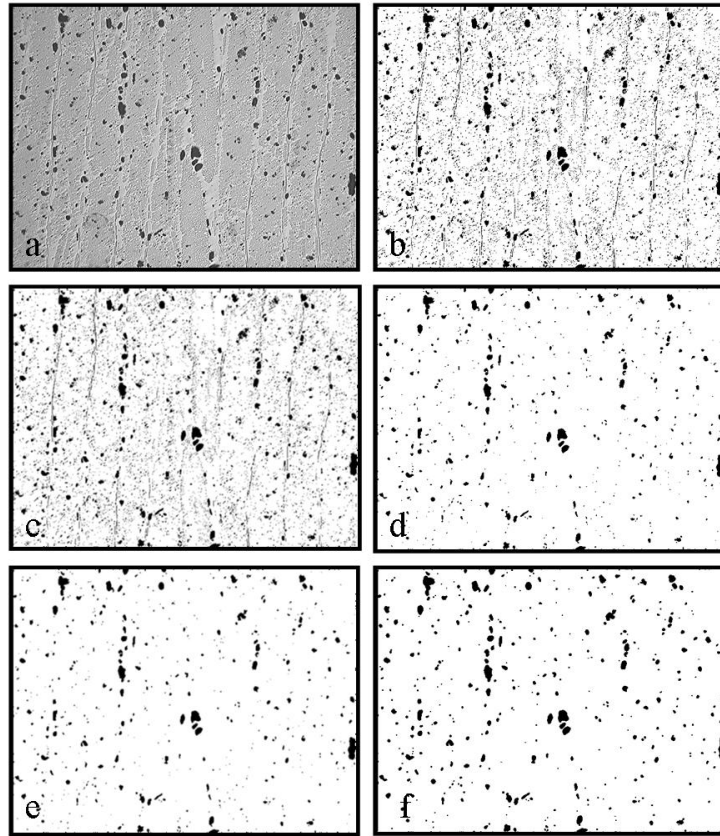
Figure 3.2   The original image (a) through the final processed image (f)
as captured from the automated process of ImageTool of a
glass/epoxy sample. Images (b, d, f) are after thresholding
while images (c and e) are after filtering steps.

The slide bar directly under the 255 on the scale is selected with the mouse and slid down
to zero. This eliminates all of the red pixels, meaning that if thresholded at this setting the
entire image would be left white. The slide bar is then slowly moved toward higher numbers
while the operator examines the original image and red pixels fill in areas that would be turned
black if thresholded at the current setting. The slide bar is moved until the red pixels fill in all
of the porosity in the image. The threshold value is recorded at this point and the *OK* button
is selected. The image shown in Fig. 3.2b is now a binary image and unless there was a very
high contrast between the porosity and the rest of the micrograph, the image will still contain
black pixels that are not actual porosity. A filtering step is applied to help eliminate the black
pixels that are not actual porosity. The *Smooth A Lot* filter is used and can be found under
the processing menu resulting in Fig. 3.2c. The image is now ready to be thresholded again
following the same procedure described earlier. This process is repeated, Figs. 3.2d-e, until

the operator is satisfied that the final binary image (Fig. 3.2f) represents only the porosity that was present in the original image. Once the average values are found from the manual thresholding process, they can be inserted into the internal script for automation of the image processing. The automatic scripts used for this experiment will process approximately 125 images per minute. Since the manual thresholding is somewhat subjective and dependent on the operator, the human factors were evaluated by comparing the image processing results obtained using the manual threshold values chosen by four individuals. Individuals were given the same set of five images and instructions on the use of the ImageTool software. They were asked to manually threshold the five images and to record their threshold values for each of the required iterations. The recorded values were then averaged and used to automate the process as would be done when following the reported procedure. The average percent porosity obtained by the four individuals was 8.4 percent and the average deviation was 0.83 percent porosity. This is approximately a 10 percent deviation from the mean value.

3.2   Results

The laboratory samples were processed first to evaluate the effectiveness of the image processing method. The G sample group has a very uniform distribution of porosity according to ultrasonic inspection results. This combined with the morphology encountered in woven lay-ups can explain the very strong correlation between the two methods shown in Fig. 3.3. Groups A, B, and D have a nonuniform distribution of porosity according to ultrasonic inspection. Since the image processing method inspects only one plane of the sample at a time, it is easy to see that there can be variations in the porosity content from one plane to the next. The cigar shaped porosity pockets encountered in the unidirectional lay-up of group A can lead to gross variations in the calculated percent porosity from the image processing method. Figure 3.4 shows the correlation of the results from the image processing and acid digestion methods for groups A, B, and D. The more evenly distributed spherical porosity elements of the typical woven lay-up described by Hsu(8) could explain why the correlation between the two methods is better for groups D and G. The results from groups E and F are shown in Table 3.2. Porosity levels obtained by the image processing method are only given for groups E and F as acid digestion values were unavailable.

Method Comparison for Group G
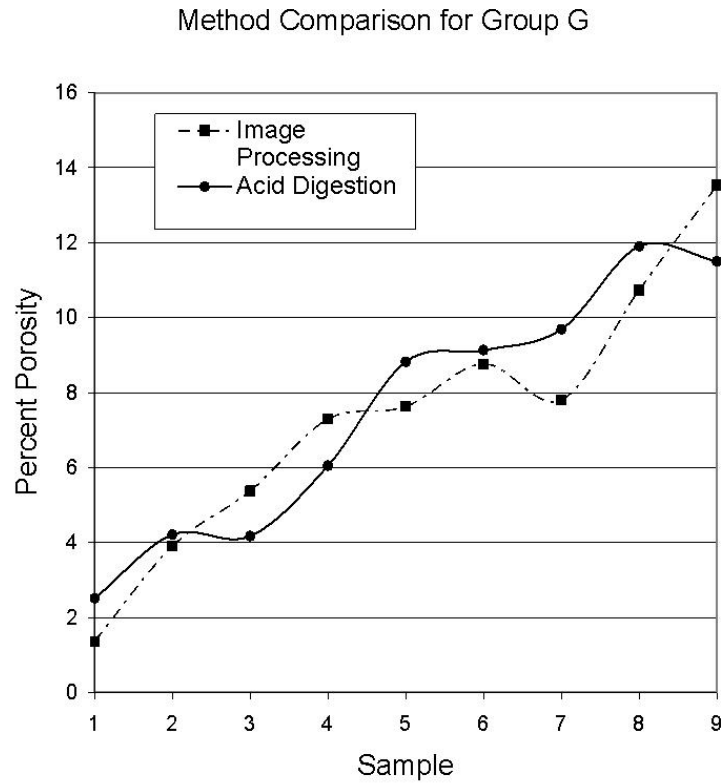
Figure 3.3   The comparison between the porosity levels obtained from the acid digestion and image processing methods on samples of group G.

Percent porosity found for groups E and F										
Group	1	2	3	4	5	6	7	8	9	10
E	8.64	13.27	7.17	5.23	6.51	11.18	9.13	8.59	3.57	8.39
F	4.30	2.96	3.26	3.37	3.56	—	—	—	—	—

Table 3.2   The porosity levels obtained from the image processing method.
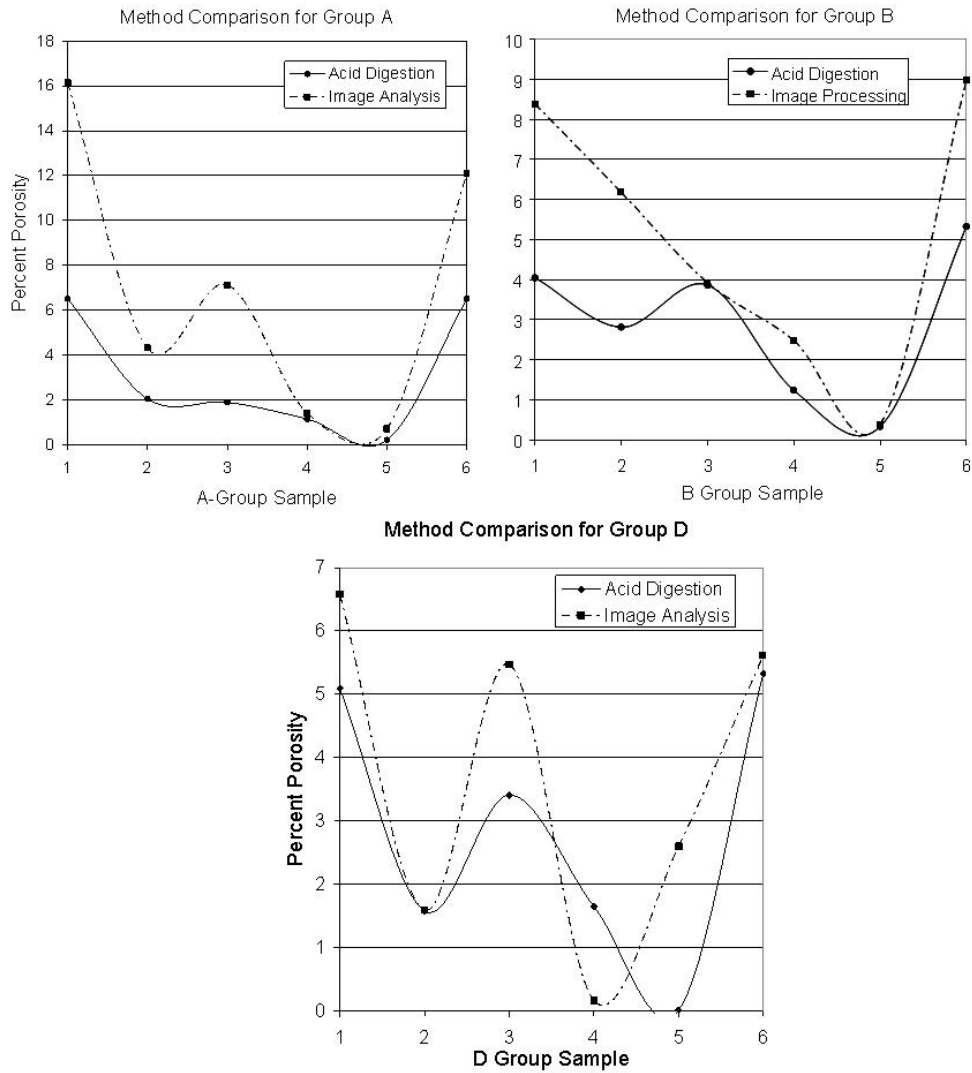
Figure 3.4   The comparison between the porosity levels obtained from acid
digestion and image processing methods on sample groups A,
B, and D.

CHAPTER 4. INSPECTION METHODS

The imaging and inspection methods utilized during this research will be discussed in the following sections. The two methods of imaging employed were the commercially available scanning frame from SONIX(13) and the Generic Scanner(GenScan) under development at CNDE. Air-coupled ultrasonics(air UT), the computer aided tap tester(CATT), and pitch-catch ultrasonics were all explored as possible inspection methods for the spar sections.

4.1 Imaging Techniques

Imaging methods are continually gaining acceptance for use on the shop floor as they offer several practical advantages over non-imaging methods. The primary advantage is that images give an overall view of the inspected part and allow the inspector to easily judge the size, shape, and location of the damage. Underlying structural features or changes in the geometry of the part often cause variations in the response from a NDE instrument, and imaging methods allow differentiation of these effects. An image is also quite useful to guide repair activities once damage is found. Images require little media space for archiving, and allow simple comparisons for growth of damage areas during service if the damage is initially below the threshold required for repair. Amplitude C-scans were used in evaluating test samples for this work and were created using three different methods. Air-coupled and pitch-catch ultrasonic measurements used the SONIX or the GenScan scanning system. To create tap test images, the Computer Aided Tap Tester was employed.

4.1.1 SONIX Laboratory Scanner

The SONIX scanning system is a three-axis, computer controlled, positioning system that can be easily programmed to rapidly inspect an area with ultrasonic transducers. The system consists of a scanning frame, a computer controlled positioning motor for each of the three scan axis, an Analog to Digital(A/D) data collection circuit board, and a scanning software program. The software contains a digital oscilloscope along with all the necessary programming and data collection utilities to collect time-of-flight and amplitude data. The SONIX scanner is capable of an xyz scan up to 48 x 24 x 18 inches. Figure 4.1 shows a screen shot of the software with a completed scan image.
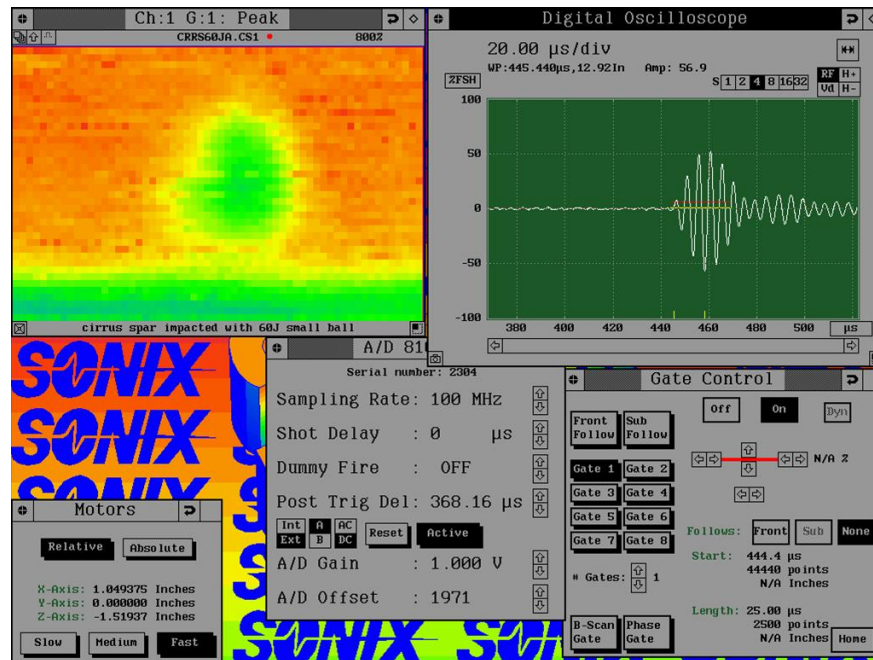
Figure 4.1   Sample display typical to SONIX scanning software.

4.1.2   Generic Scanner

The Generic Scanner or GenScan is a manual scan system under development at CNDE that combines simple and inexpensive position encoding hardware, hand-held portable inspection instruments, and a computer with software that enables the production of C-scan images(6). A core concept of this development is to use NDE equipment already in use by and familiar to inspectors, thus minimizing inspection procedure changes. A minimal selection of scan sizes and data collection settings are utilized to reduce the training required to operate the unit. To date, the system has been deployed using portable ultrasonic flaw detectors, bond testers and eddy current units. The system utilizes an innovative feature that allows pixel size changes on-the-fly, which greatly reduces the scan time compared to other manual scanner systems. After the scan area size is set by the user the software displays an all red image of the chosen dimension. As the transducers are manually moved about the scan area the red pixels are replaced by grayscale pixels that represent the amplitude or time of flight data at the reported position. The adjustable pixel size allows a rapid preliminary scan to be done at a large pixel size. Then, if an area of suspicion arises it can be rescanned at a smaller pixel size to increase the resolution of the desired area. Refining only the areas of interest saves time over scanning the whole area at a high resolution setting. The GenScan concept greatly reduces equipment costs compared with commercial automated scanners designed for field use when C-scan capabilities are needed.

During this research, GenScan was used in conjunction with a Panametrics Epoch 4 flaw detector, in both TTU and pitch-catch mode, with either the Ultran GMP transducers or the miniature potted Rayleigh wave transducers. Gated peak amplitudes were detected by the instrument. The detected amplitude values were transmitted along with the position data from the encoder system, via serial connections to the computer running the GenScan software. This information is compiled by the software to create a C-scan image similar to that shown in Fig. 4.2.
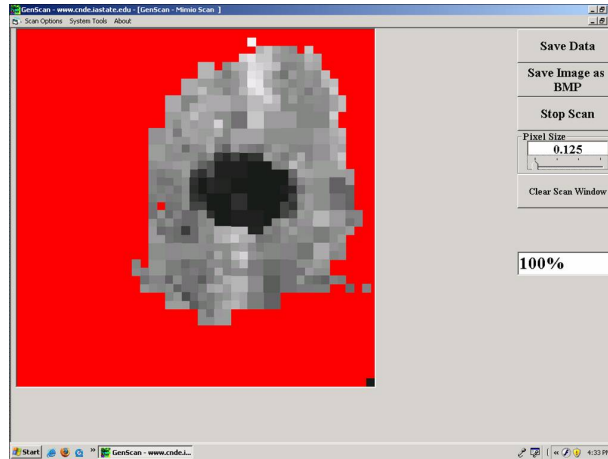
Figure 4.2   The GenScan image of an impact damage as seen by the user.

4.2   Air Coupled Ultrasound

When choosing to utilize air coupled ultrasound over traditional ultrasonic methods such as immersion testing for nondestructive evaluation techniques there are several items to consider. There is a large impedance mismatch between air and solids which creates energy transfer problems between the two media. The impedance ratio of carbon fiber reinforced panel(CFRP) to water is 3 to 1 while the impedance ratio of CFRP to air is 10000 to 1. Using the formulas for the reflection and transmission coefficient,(equations 4.1 and 4.2), we find that 99.96 percent of the energy is reflected at an air and CFRP interface.

$$\alpha_r = \left[\frac{Z_2 - Z_1}{Z_2 + Z_1}\right]^2 \tag{4.1}$$

$$\alpha_t = \frac{4Z_2 Z_1}{(Z_2 + Z_1)^2} \tag{4.2}$$

Where α_r and α_t are the reflection and transmission coefficients, respectively, and Z_1 and Z_2 represent the impedance in materials 1 and 2.

Even with the high reflection coefficient resulting from the large impedance mismatch, better transducer technology and modern electronics have made the use of air-coupled ultrasound possible. The advances in transducer technology, such as the Gas Matrix Piezoelectric(GMP) transducers by the Ultran Group and the piezoceramic transducers with multiple matching layers from QMI, have increased the efficiency of energy transfer to and from the transducer with the surrounding air. Unlike piezoceramic transducers that are constructed from a solid piezoceramic crystal, the GMP transducers use a matrix of piezoceramic rods surrounded by air. The acoustic impedance of this composite matrix is reduced, providing a better match to air than that of a standard transducer. The addition of one or more matching layers with an intermediate acoustic impedance, an impedance between that of the ultrasonic source and the air couplant, will further increase the efficiency of energy transfer.

The three ultrasonic systems used during this research were the Panametrics Epoch 4 coupled with the Ultran GMP transducers, the Panametrics 5058 pulser-receiver coupled with the Ultran GMP transducers, and the QMI SONDA-007CX Airscan system utilizing QMI transducers. The three systems are all relatively low cost, highly portable, and are equipped to output their data to either the SONIX or GenScan system for imaging.

The Epoch 4, shown in Fig. 4.3, is a hand-held, easily portable, ultrasonic flaw detector that is used by CNDE in the lab and in the field on a regular basis(14). This flaw detector is capable of producing a spike or a tunable square wave pulse. The square wave pulse is used for the inspection of the spar specimens. To provide adequate power to the GMP transducers for through transmission of the spar sections, the Epoch 4 is set to the maximum energy setting with a damping level of 50 ohms. The filters are set to best accommodate the 200 kHz transducers.

Figure 4.3   The Panametrics Epoch 4 shown with the Ultran GMP transducers performing an A-Scan through GS1.

The 5058 pulser-receiver from Panametrics has a built in preamplifier with high and low pass filters. This piece of laboratory grade hardware must be paired with an oscilloscope to view the resulting waveforms produced while inspecting a component. The pulser-receiver can be used to power the Ultran transducers as seen in Fig. 4.4.
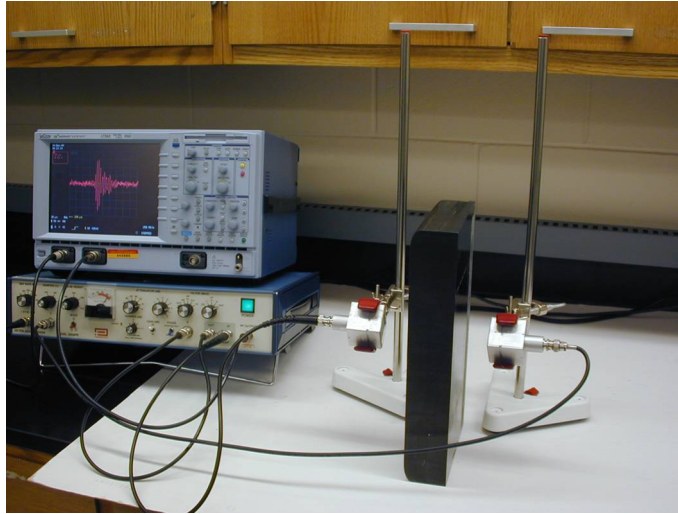
Figure 4.4   The 5058 pulser-receiver with the GMP Ultran transducers and
the LeCroy oscilloscope.

The QMI SONDA-007CX Airscan system (5) is shown in Fig. 4.5. This is a stand alone system that houses the pulser-receiver, oscilloscope, and keypad controls in one small unit. The QMI system utilizes all ceramic transducers with a preamplifier built into the receiving transducer and offers the ability to individually tune each transducer to optimize the signal.

Figure 4.5   The QMI air-coupled ultrasonic system.

C-scan images previously produced utilizing the QMI system are shown below in Fig. 4.6 and Fig. 4.7. These images are shown to demonstrate that the capabilities of air coupled ultrasound have already been examined in materials similar to those used in light composite aircraft(15; 16).
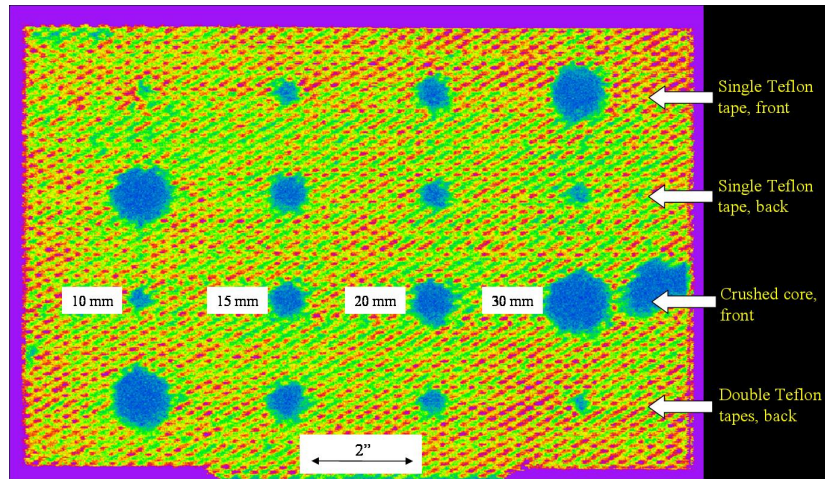
Figure 4.6   Image produced from QMI 400 kHz focused transducers through a Kevlar/Nomex honeycomb sandwich composite.
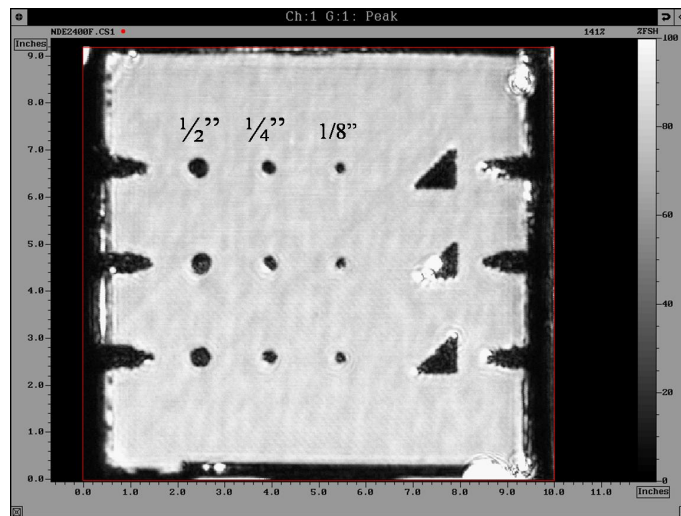
Figure 4.7   C-scan image with engineered defects produced from QMI 400 kHz focused transducers through a 10-ply solid laminate.

4.3   Computer Aided Tap Tester

The computer aided tap tester by Advanced Structural Imaging Inc. is an instrumented tap testing unit that creates C-scan type images(3). The user tap tests a composite structure with a device that contains an accelerometer. This is an inexpensive technology previously developed at CNDE during an FAA funded project. This method of inspection may be useful to further classify a damaged region previously flagged by an air-UT scan. This inspection can be done on small areas by hand, one tap at a time, or on larger test areas using a cart that allows rapid tapping with minimal inspector effort. To use this system the inspector specifies the size of the area to be tested, then taps the tapping device in each cell of a grid placed over the test area. The grid is a mesh of square cells printed on a thin transparent plastic sheet. The size of the mesh depends on the required resolution of the scan area. Data acquisition software captures the contact time, or tap duration, between the probe and the test specimen for each tap at each location. The tap duration, measured with an accelerometer, can be directly correlated to the out-of-plane stiffness of the part if the mass of the tapper is known. This information is displayed in a C-scan image which allows the user to see the whole test area while interpreting the scan information. The basic CATT system is shown in Fig. 4.8. This system works well on sandwich composite structures and thinner sheets of composite material. This technique may be useful on the thin web portion of the composite spar. A complete description of the physics behind the tap tester can be found in Ref. (17).
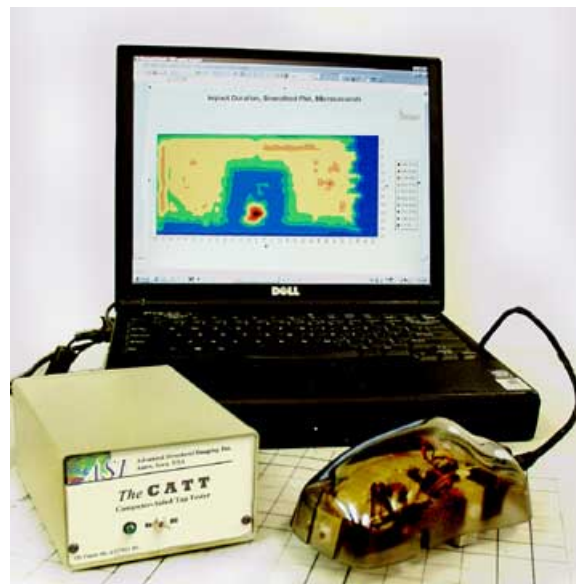
Figure 4.8   The CATT system shown with a sample image visible on the laptop screen.

4.4   Pitch-Catch Ultrasound

The pitch-catch method is being experimentally explored by CNDE as a possible solution to the common problem of testing the unfavorable geometry found on many aerospace structures. Often the part geometry does not provide the flat back surface necessary for normal incidence pulse-echo inspection; if this is the case, pitch-catch ultrasonics may be useful since they do not use a backwall reflection. The pitch-catch technique uses small potted angle beam transducers originally designed to create Rayleigh waves in steel structures. Since the critical incident angle to create Rayleigh waves is not reached when these transducers are used on a composite material, they produce refracted longitudinal or shear waves inside the laminate. When two of these transducers are used as shown in Fig. 4.9, only the area near the intersection of the transmitting and receiving beams is sampled. With the transducers arranged in the nose-to-nose fashion they have a footprint of 1.5" x 0.25". This unsymmetrical footprint can cause elongation of defects in the scan images. The pitch-catch method has been used to detect embedded objects as well as impact damages and is especially useful when the defect is near the surface. This method, when coupled with GenScan, becomes a powerful technique for creating a C-scan image for interpretation by the inspector.
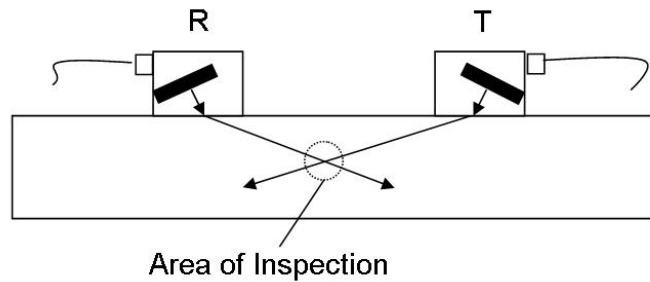
Figure 4.9   Sketch of the pitch-catch system and the resulting area of inspection where T is the transmitter and R is the receiver.

CHAPTER 5.   AIR COUPLED ULTRASOUND

The experimental work with air-UT was divided into four main categories; the fundamentals, the acrylic ply drop-off sample, the glass fiber specimen, and the carbon fiber specimens. The fundamental experiments consisted of the inspection of some of the defects that were expected to be encountered during the testing of the main wing spar. Examples of the inspected defects include impact damage and foreign object inclusions.

5.1   Impact Test Panel (A-20)

The first fundamental experiment inspected an impact damaged carbon fiber panel provided by Cirrus during the kick-off meeting on December 20, 2005. The A-20 test panel measured 4.0" by 6.5" with a thickness of 0.375" and had been impacted by a hammer blow of unknown force by Cirrus. The objective was to verify that air coupled ultrasound could be used to identify the defect. An amplitude C-scan of the panel was made with the QMI and SONIX system. The set-up is shown in Fig. 5.1. The panel was scanned with 120 kHz and 400 kHz focused transducers.
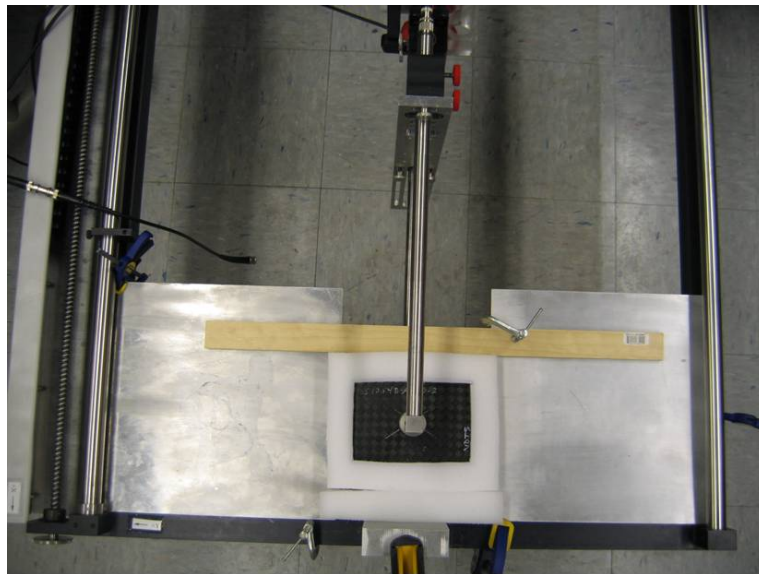
Figure 5.1   The A-20 impact panel set up in the SONIX scanning frame.

The amplitude C-scan made with the 120 kHz transducers depicted the impact damaged area as a low intensity region as shown in Fig. 5.2, meaning the damage was attenuating the ultrasound passing through the test panel. The amplitude C-scan colors represent the intensity of the sound reaching the receiver. The cause of the high amplitude square box that surrounds the impact damage is unknown. The scan results using 400 kHz transducers, Fig. 5.3, depicted the impact damaged area as a low intensity region as well.
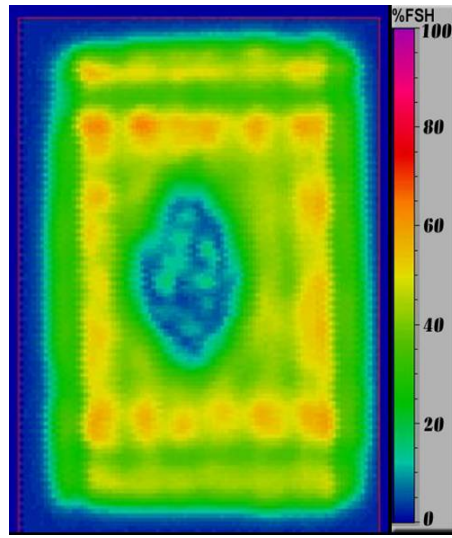
Figure 5.2   The 4.5" by 6.5", 120 kHz scan image of the A-20 impact panel.
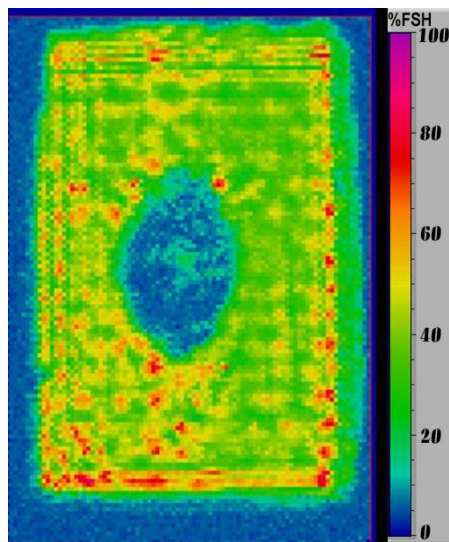
Figure 5.3   The 4.5" by 6.5", 400 kHz scan image of the A-20 impact panel.

5.2   Grafoil and Teflon Foreign Object Test Panel

The foreign object test panel was a carbon fiber plate that had six-one inch square inserts of Grafoil and Teflon embedded in the layup (GT panel). The goal of this experiment was to see if air-UT could detect this type of object. The scans were made with the SONIX scanning frame and the QMI system and the set-up is shown in Fig. 5.4. Images were made with the 120 kHz and 400 kHz focused transducers.
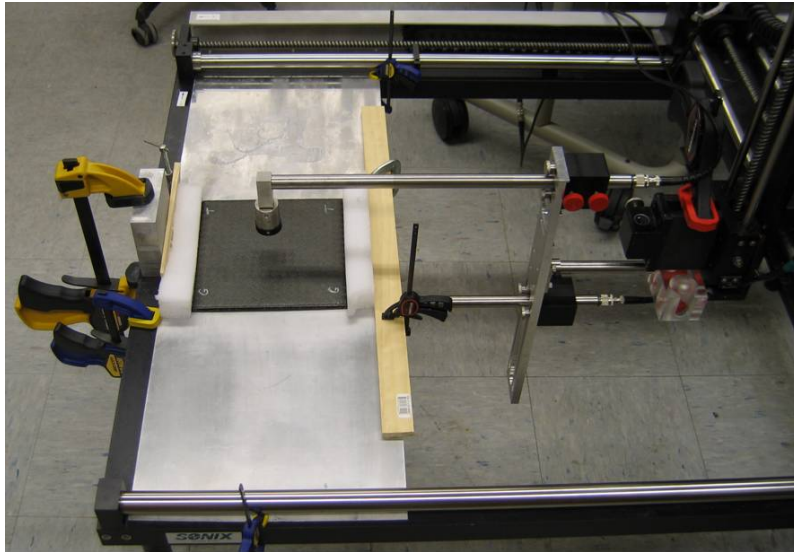
Figure 5.4   The scan setup of the GT foreign object panel.

The images produced from the amplitude C-scans were very interesting. The inserts were intended to simulate a delamination or an embedded foreign body and would be expected to show as a region of lower sound transmission. This was indeed the case with the Teflon inserts but the opposite was true with the Grafoil inserts. The Grafoil inserts show up in the scan as a region of higher through sound transmission as seen in Fig. 5.5. This phenomenon has been encountered in past research by Kommareddy (16) of CNDE and Schindel (18) of Queens University. Schindel used resonance as the explanation of this occurrence while Kommareddy used theory that relates to interference or the so-called Poison's Bright Spot. Another important factor is that the bonding conditions of Teflon and Grafoil to CFRP could be different. This phenomenon could make identifying a damaged region more difficult during inspection if defects could show up as both high or low intensity regions.

The images produced with both the 120 kHz and the 400 kHz frequencies were very similar. They both show the Grafoil inserts as higher intensity regions than the Teflon inserts. The 400 kHz scan does show more detail of the ply orientation or weave of the fabric as seen in Fig. 5.6. This is common when using a higher frequency since the shorter wave length increases the spatial resolution of the scan.
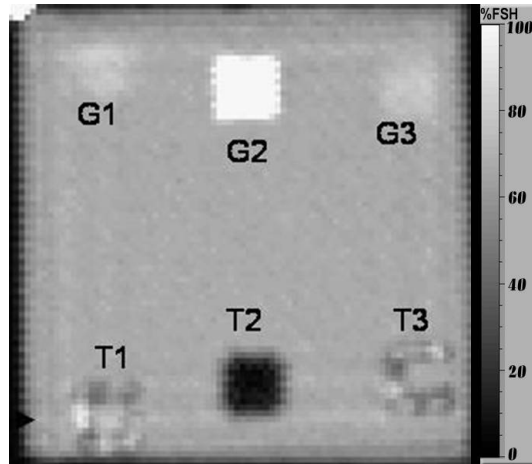
Figure 5.5   8.0" by 8.0" amplitude C-scan image from QMI 120 kHz transducers showing Grafoil(G) and Teflon(T) one inch square embedded defects.
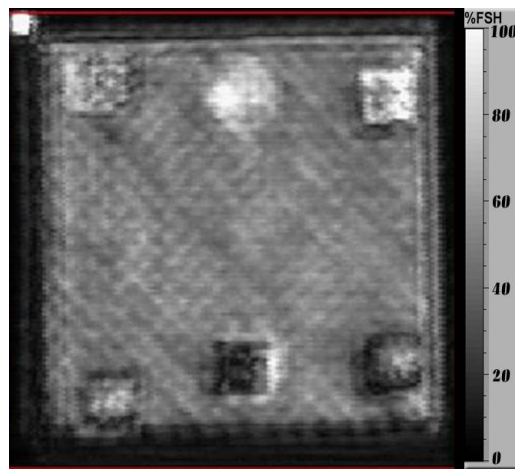
Figure 5.6   Amplitude C-scan image of GT panel with 400 kHz transducers.

5.3   Acrylic Spar Mock-up Sample

A model of the spar web section was made from acrylic to have an isotropic specimen for study of the geometric effects of the ply drop-off region on the ultrasonic wave. The model simulated the thin web, the ply drop-off region, and the thick web area. Figure 5.7 shows a photo of the acrylic model.
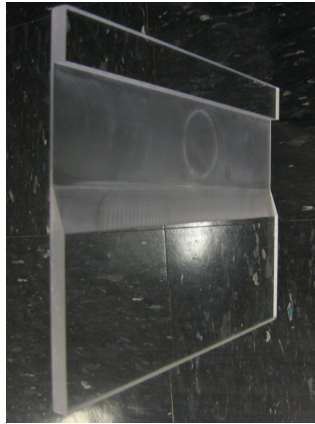
Figure 5.7   The acrylic web model used for testing.

Amplitude C-scans were made with the Epoch 4 and the Ultran 200 kHz transducers with the SONIX scanning frame. The first scan image was made with the receiver tilted nearly normal to the ply drop-off, 12.5 degrees off vertical, shown in Fig. 5.8. This maximizes the signal through the ply drop-off area but slightly reduces the effective signal through the thick and thin web, see Fig. 5.9.
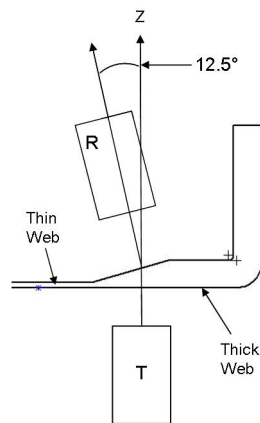
Figure 5.8   The receiver tilted to 12.5 degrees off vertical for increased ply
             drop-off penetration.
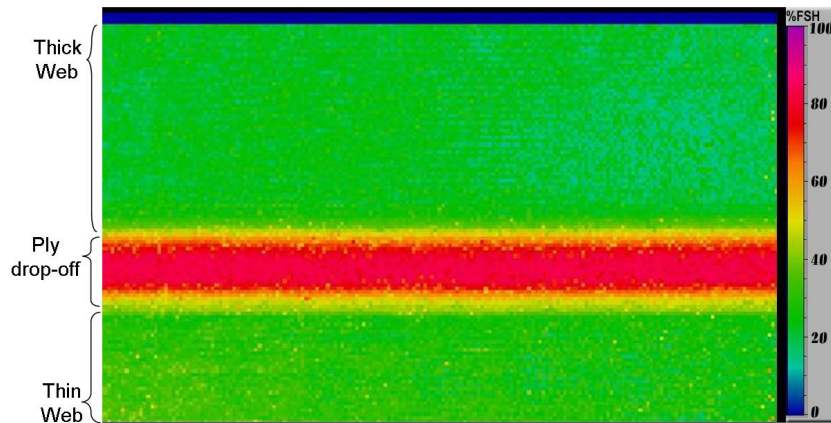
Figure 5.9   C-scan of the acrylic test panel using the Epoch 4 with the
             receiver tilted to 12.5 degrees.

Since tilting the receiver to 12.5 degrees maximized the signal in the ply drop-off region but reduced the signal in the thick and thin web, it was decided to find a tilt angle that would give good signal penetration through all three web areas. It was found that by tilting the receiver two degrees off the normal vertical axis, good signal strength could be obtained in all three areas of the web. The image produced from this setup can be seen in Fig. 5.10. The scanning of the acrylic spar model provided insight into possible scanning techniques for use in testing the carbon spar samples.
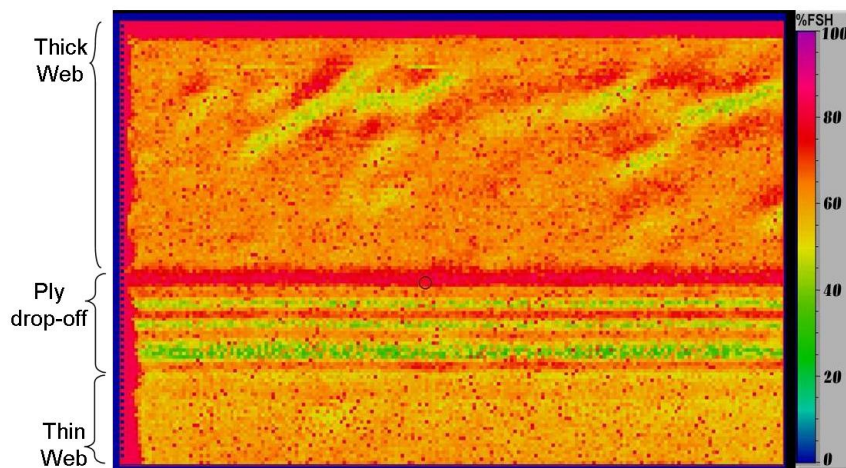
Figure 5.10   Image of the acrylic sample with receiver tilted 2 degrees off
              normal.

5.4 Glass Spar

The Epoch 4 flaw detector was used to power the Ultran 200 kHz transducers for a TTU test on several regions of GS1. The tests were performed in the cap, thin web, and radius of the spar. All three positions produced a suitable signal with good signal to noise ratio as seen in Fig. 5.11. This test shows that a suitable signal for scanning can be obtained from such low cost equipment(19) as the Epoch 4.
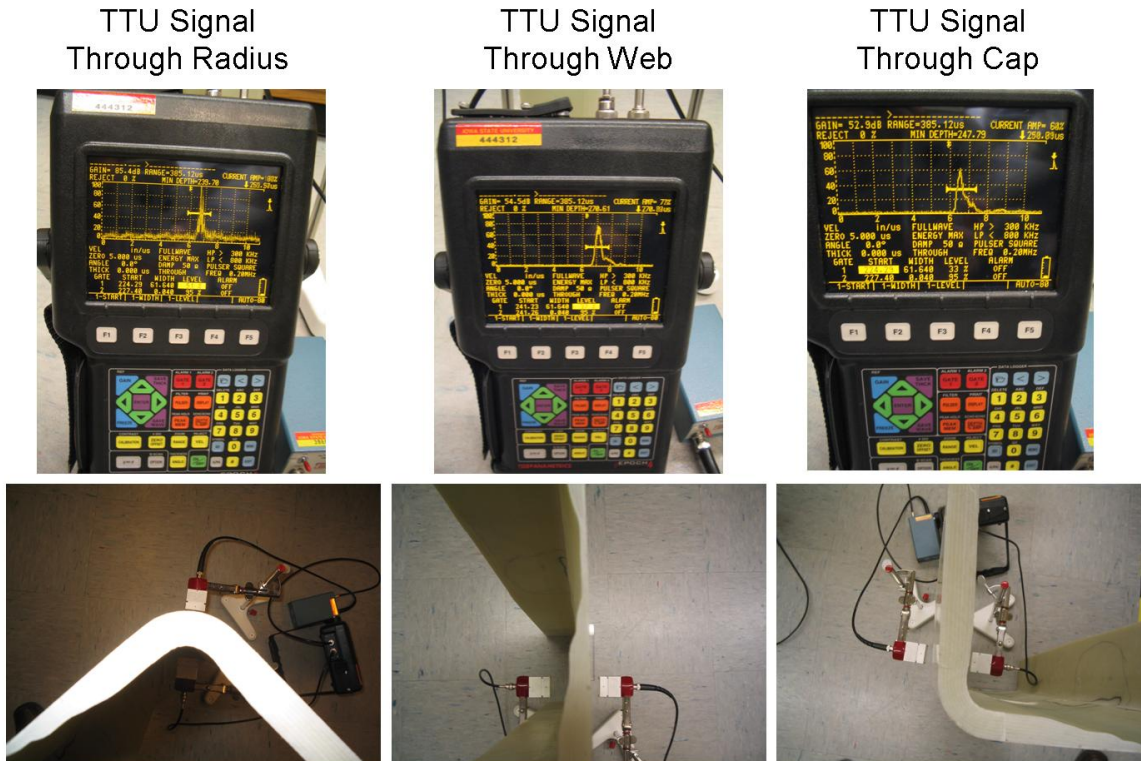
Figure 5.11   Signal produced through three critical portions of the GS1 spar
using the Epoch 4.

The GS1 spar was set up in the SONIX scanning frame to be scanned with the Ultran transducers at a frequency of 200 kHz as demonstrated in Fig. 5.12. The transducers were powered by the Panametrics 5058 pulser-receiver with the Panametrics preamp in the receiver line. The amplitude C-scan image produced from the web of GS1 is shown in Fig. 5.13. The six circular holes show as high intensity regions in purple. There seems to be banding along the ply drop-off areas and a ply overlap is visible crossing the thin web at a 45 degree angle to the right of the large hole.
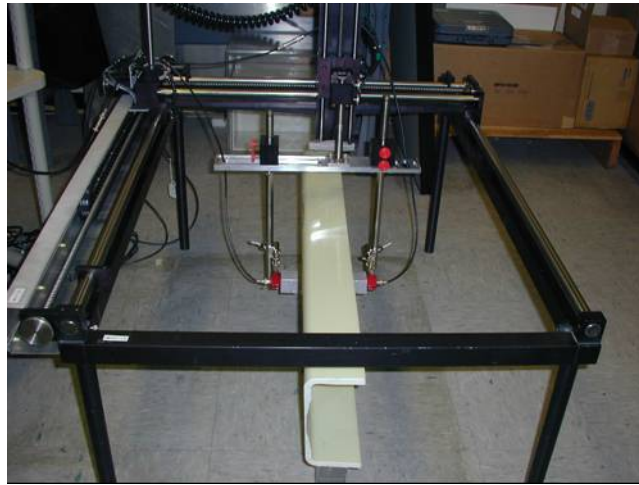
Figure 5.12   Setup used to scan the whole web of GS1.
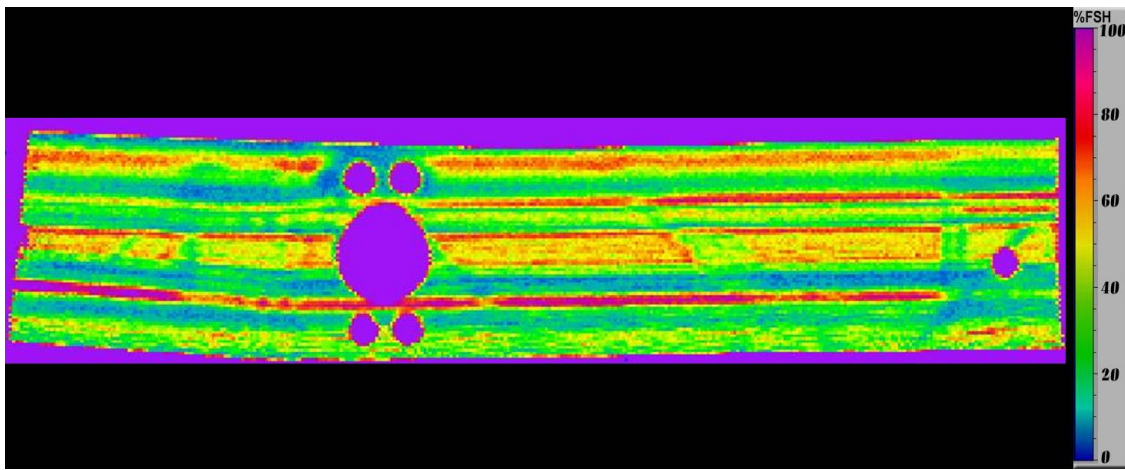
Figure 5.13   The C-scan image produced from the whole web of GS1. This
                33" by 10" scan of GS1 shows the two ply drop-off regions with
                the machined holes as well.

5.5   Carbon Spars

5.5.1   Carbon Spar 1 (CS1)

CS1 was supplied with nine impact damaged areas induced by Cirrus. This sample was also damaged in the web section by a destructive joint pull-off experiment performed by Cirrus prior to supplying the spar to CNDE. The impact damages were induced by dropping a weight from a known height to impart the desired amount of energy to the spar through an impactor with a one-half inch diameter tip. The true amount of energy transfered to the part can be found by recording the rebound height of the impactor. The initial drop height minus the rebound height will give the height correlating directly to the amount of energy transferred to the part. No information was provided by Cirrus on rebound of the impactor used on CS1 so the impact energy labeled on each impact site may be higher than the actual energy received by the part. The impacts were induced in either the supported or unsupported state. The supported state had a metal backing plate that was placed directly behind the impact site. This provided direct support of the area during the impact process. Three impacts were done on the thin web with energies of 10, 20, and 30 Joules each. Three more impacts were induced on each cap at the same energies with one cap in the supported state and the other in the unsupported state during the impacts. It was believed that the previous pull-off damage would not make this inspection impossible, although it was expected to make the C-scan image more difficult to interpret.

The SONIX scanning system was utilized with the QMI system to make the first air UT images of the web area as shown in Fig. 5.14. The image produced showed the three impact damages and some of the damage caused by the joint pull-off testing. Interestingly, these defects again appeared as an area of higher transmission, note Fig. 5.15. This is similar to the results on the Grafoil inserts described previously in section 5.2.

Figure 5.14   The scanning setup used for the CS1 wing spar section.
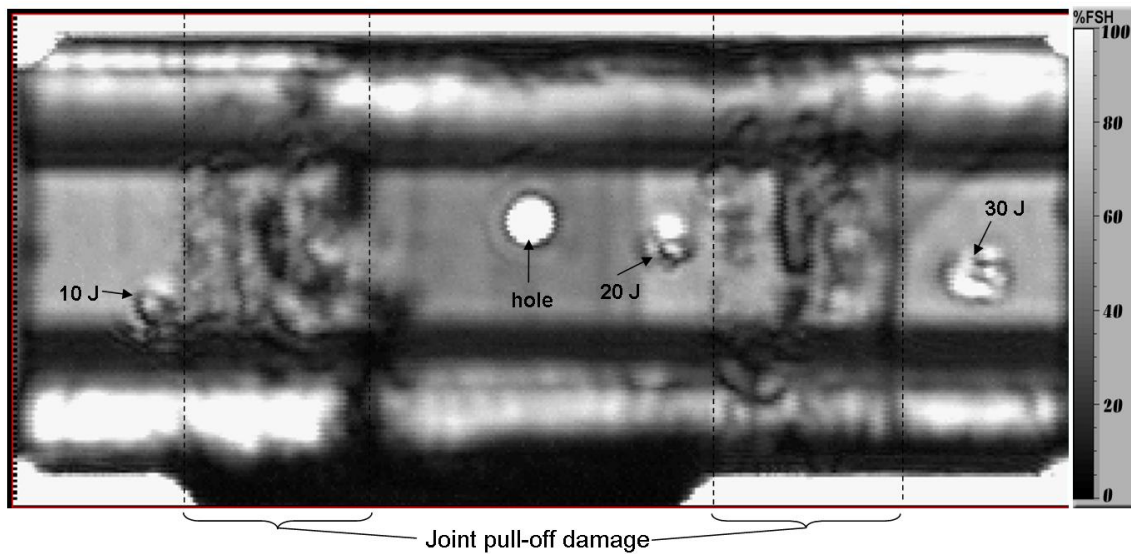
Figure 5.15   The 18" x 8.5" amplitude C-scan image produced from the
web of CS1 with the QMI 120 kHz focused transducers.

After the preliminary scans of CS1 in the condition received were complete, the loose layers
in the pull-off damage region were cleaned up to reduce their effects on the C-scan images.
The central portion of the web surrounding the hole was virtually undamaged, but in both
directions extending toward the ends of the spar, there was considerable damage in the web as
many plies were pulled away as a result of the joint testing performed by Cirrus. The inside
web surface of the spar was sanded extensively to remove the damage caused by the destructive
joint testing. After the clean up process the spar was scanned again using the same setup as
before shown in Fig. 5.14 . This setup was used to create the C-scan images for 120 kHz (Fig.
5.16), 225 kHz (Fig. 5.17), and 400 kHz (Fig. 5.18). Note that the pull-off damage is less
visible in Fig. 5.16. Figure 5.18 depicts the impact damage areas in the thin web as a lower
intensity region but the overall lower amplitude appearance of the C-scan indicates that the
400 kHz transducers are too high of a frequency for good penetration of the CS1 spar. The
flat web surface of the spar is relatively easy to scan except for the ply-drop off area. This
area presents a challenge due to the angled geometry.
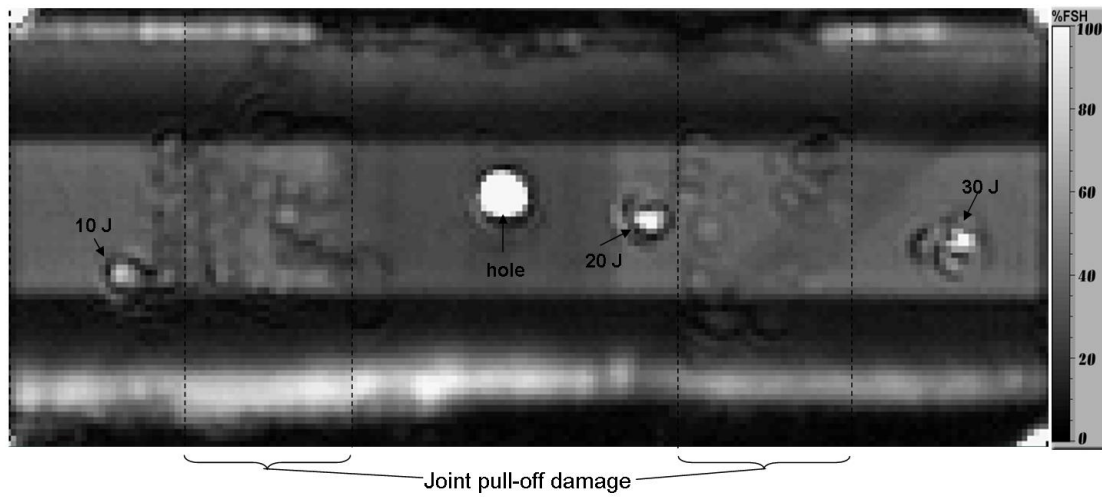
Figure 5.16   The 18" x 8.5" C-scan of CS1 after the web cleaning using the QMI 120 kHz focused transducers.
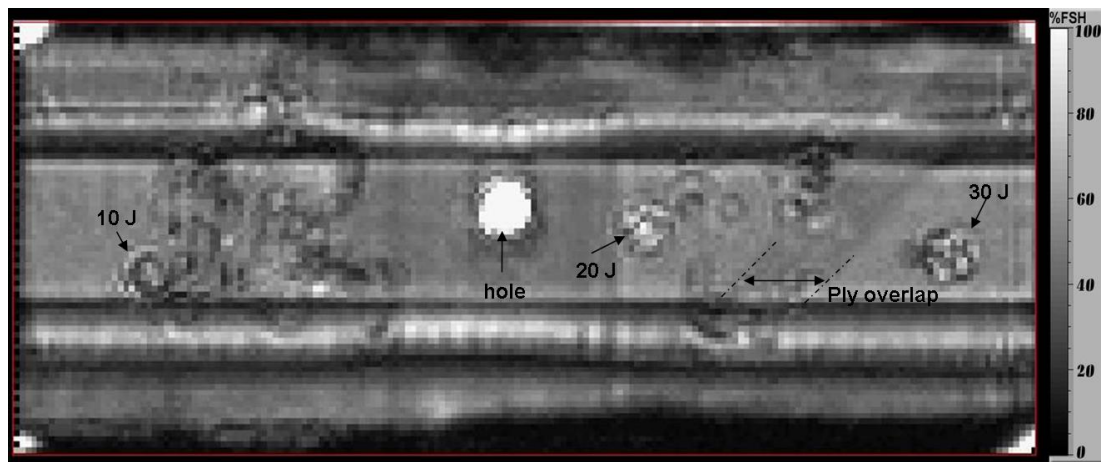
Figure 5.17   The 18" x 8.5" C-scan of CS1 after cleaning using the QMI 225 kHz focused transducers.
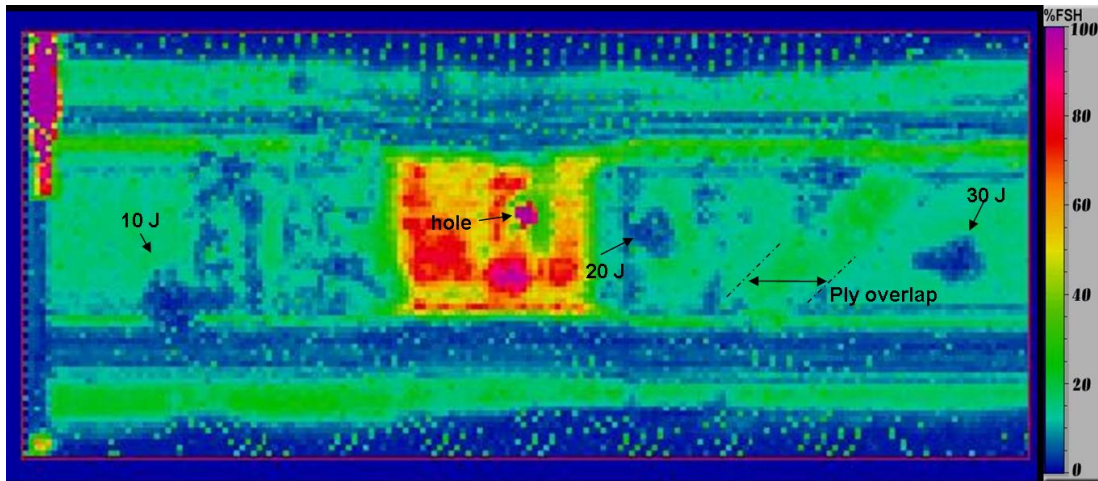
Figure 5.18   The 18" x 8.5" C-scan of CS1 after cleaning using the QMI 400
                kHz focused transducers. The high amplitude central portion
                could be a result of resonance.

5.5.2 Carbon Spar 2 (CS2)

The second carbon spar (CS2), was provided undamaged to CNDE at the end of July,
2006. C-scan images were produced with the SONIX system coupled with both the 5058
pulser-receiver and the QMI system to have baseline images for reference.

Figure 5.19 is an amplitude C-scan of the undamaged CS2 spar section. The green spot in
the center of the web is a hole plugged with foam. The web is much more uniform than the
CS1 sample that had ply pull-off damage. The edge effects along the axial edges seem to be a
reflection disturbance as the transducers approach the cap. This scan was made with the 200
kHz Ultran GMP transducers powered with the 5058 Panametrics pulser-receiver. Notice that
this sample is quite uniform which is good for detecting induced impacts. Some ply overlaps
are also visible in the C-scan.
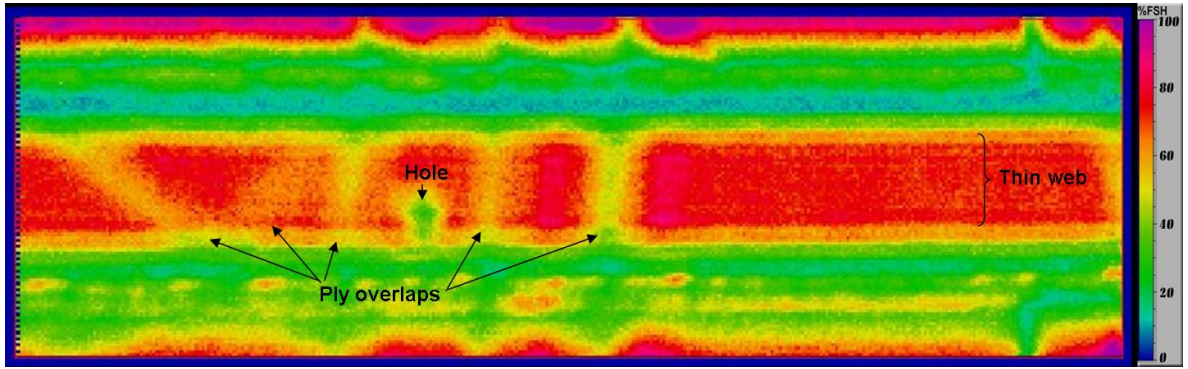
Figure 5.19   The 18" by 5.5" C-scan image of the undamaged CS2 carbon
spar. Notice all of the ply overlaps in the thin web.

Once the preliminary scans were produced, CS2 was damaged by the same method as
CS1. The impactor was dropped in a transparent acrylic tube with distance graduations and
the rebound of the impactor was recorded with video equipment. The rebound height of the
impactor was obtained from video footage and used to more accurately measure the amount
of energy induced into the spar. The information on each impact site is shown in Table 5.1.
All impacts were done in the supported state except for the 30U impact. The impacts labeled
with R had their rebound height documented by video. The location of each impact is listed
as being in either the thin web(Tnweb), thick web(Tkweb), or the ply drop-off(PDO). The
drop(D) and rebound(R) heights and energies are listed.

CS2 Impact Data						
Site	Loc.	D.Height(in)	R.Height(in)	D.Energy(J)	R.Energy(J)	Energy(J)
30U	Tnweb	27.61	NA	30.00	NA	NA
30	Tnweb	27.61	NA	30.00	NA	NA
40	PDO	36.82	NA	40.00	NA	NA
50	Tkweb	46.02	NA	50.00	NA	NA
20R	Tnweb	18.41	6.50	20.00	7.06	12.94
30R	Tnweb	27.61	5.25	30.00	5.70	24.3
40R	PDO	36.82	5.50	40.00	5.98	34.02
50R	Tkweb	46.02	10.50	50.00	11.41	38.59

Table 5.1   The details of the damage induced on CS2.
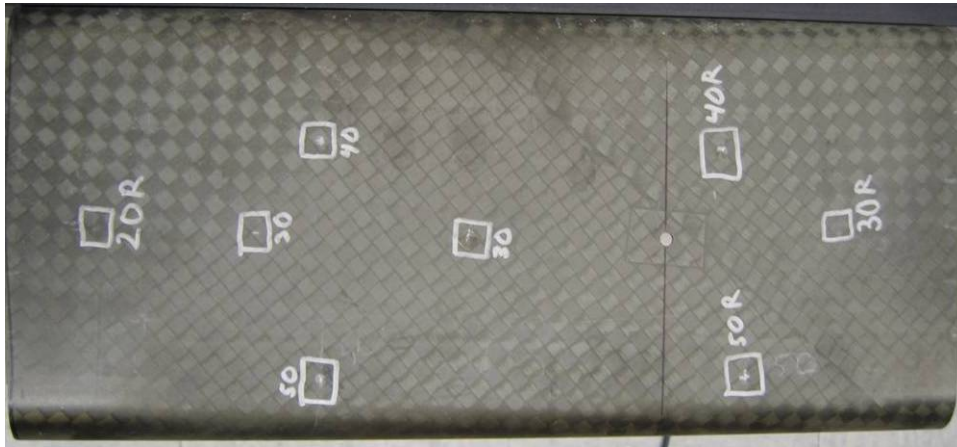
Figure 5.20   The impact damaged CS2 carbon spar.

The damage layout can be seen in Fig. 5.20. After damage, amplitude C-scan images of the CS2 spar were produced with the QMI coupled with the SONIX automated scanner and the Epoch 4 coupled with the GenScan manual scan system. The QMI scans were produced at three different frequencies of 120, 225, and 400 kHz. The 120 kHz (Fig. 5.21) and the 225 kHz (Fig. 5.22) amplitude C-scans were very informative and easy to interpret. All eight of the impact damages were visible along with the ply overlaps in the thick and thin webs. These features are labeled in both figures for easy identification.
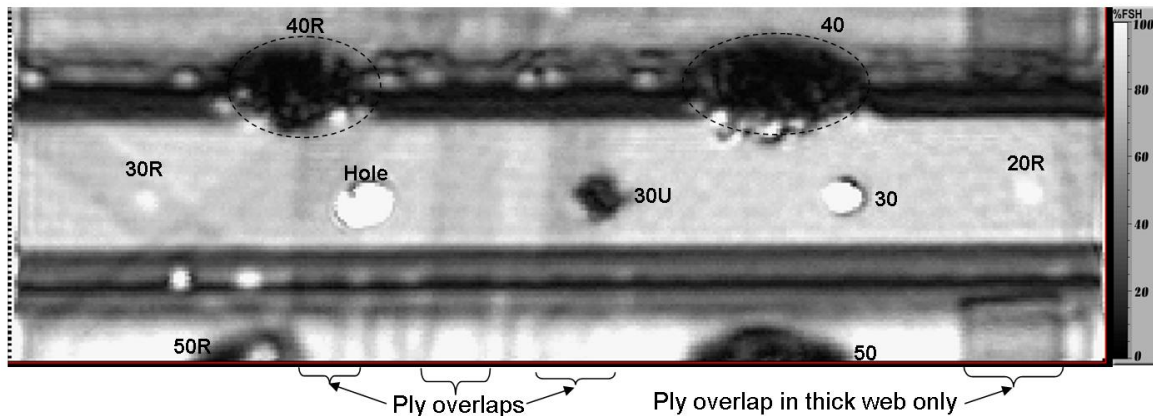
Figure 5.21   The 18" by 5.5" C-scan image of the damaged CS2 carbon spar with the QMI 120 kHz transducers.

Figure 5.22   The 18" by 5.5" C-scan image of the damaged CS2 carbon
spar with the QMI 225 kHz transducers.

The amplitude C-scan of CS2 from the QMI system with the 400 kHz transducers is shown in Fig. 5.23. The image shows the same features as the lower frequency scans but the features are harder to distinguish from the background. The 400 kHz transducers lack the penetration power of the lower frequency transducers.
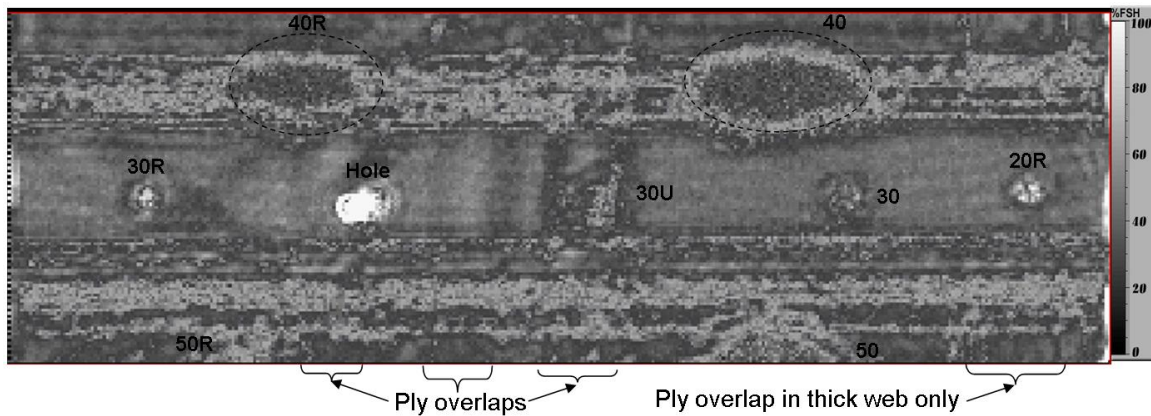
Figure 5.23   The 18" by 5.5" C-scan image of the damaged CS2 carbon
spar with the QMI 400 kHz transducers.

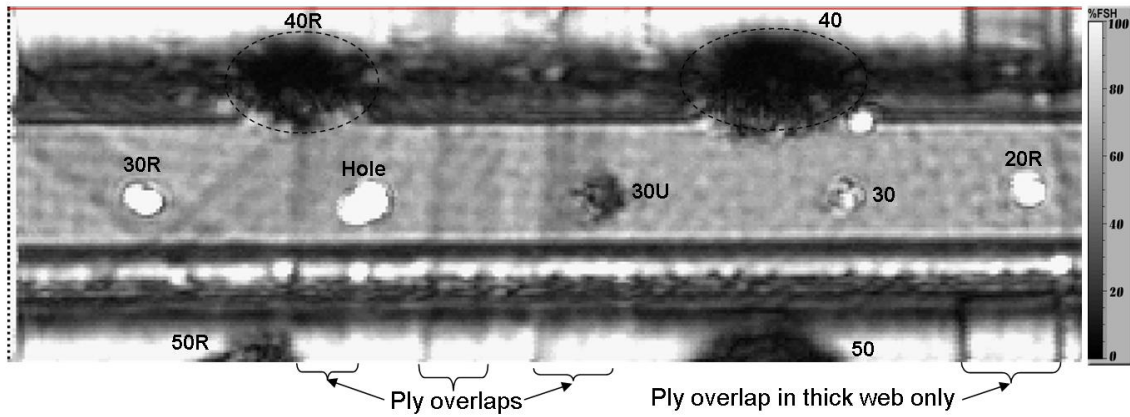The last amplitude C-scan of CS2 was created from the Epoch 4 coupled with the GMP Ultran 200 kHz transducers and the GenScan manual scanner. The C-scan was done using a lightweight and portable yoke to hold the Ultran transducers and is shown in Fig. 5.24.
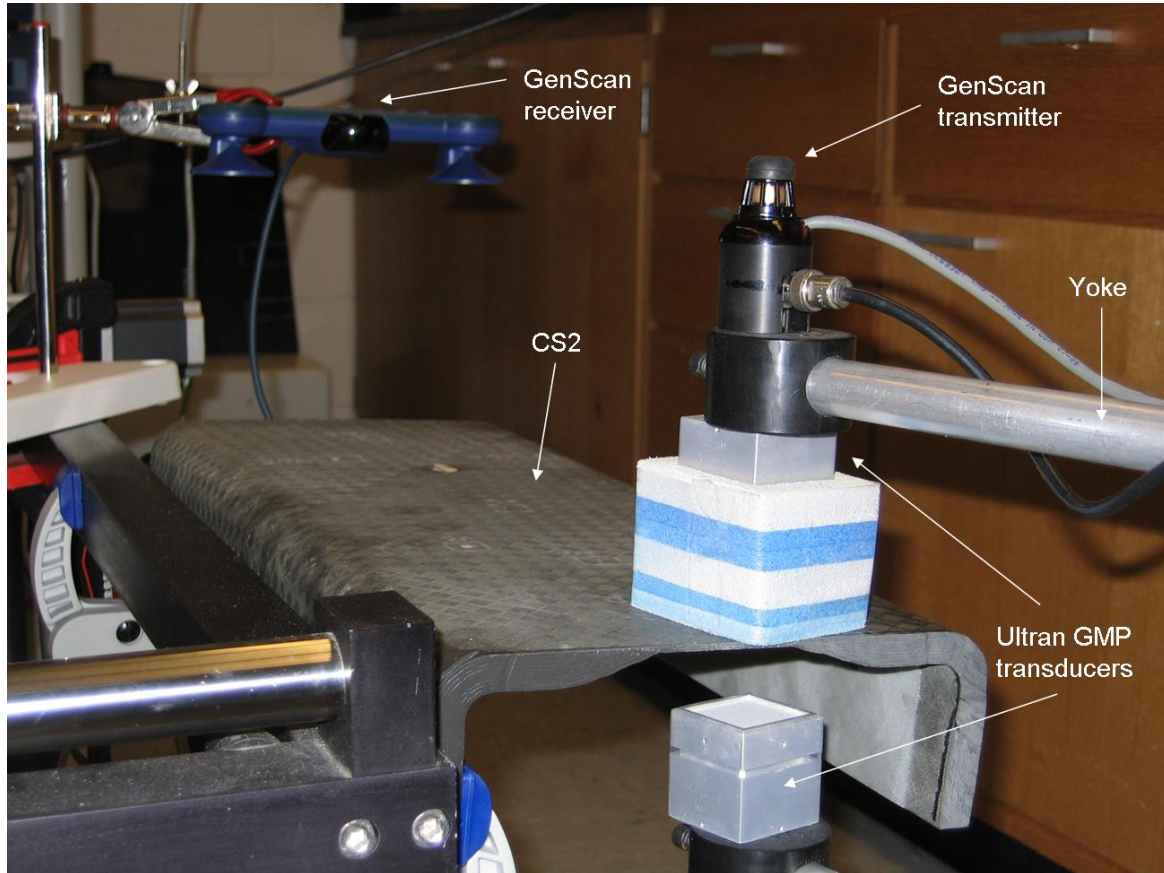
Figure 5.24   The setup of the 200 kHz Ultran GMP transducers using the GenScan system on CS2.

The C-scan in Fig. 5.25 from the 200 kHz GMP transducers shows many of the same features as the earlier scans. All of the impact damages are visible except for one in the thin web. Also seen are the damages in the ply drop-off and the thick web as well as the ply overlaps. The features have been labeled as before to help identify their location. The GenScan image is harder to interpret than the QMI C-scan images at this time. The GenScan is still under development and there are continuous advancements in the image quality that the GenScan is capable of producing.
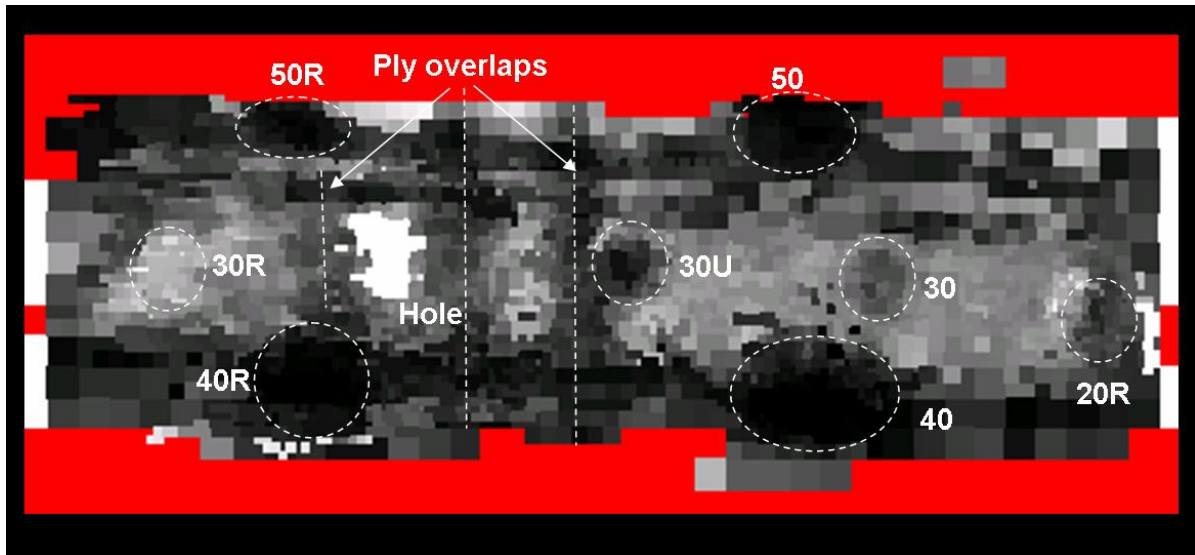
Figure 5.25   The 18" by 5.5" C-scan image of the damaged CS2 carbon spar
with the Epoch 4 and the 200 kHz Ultran GMP transducers
using the GenScan system.

CHAPTER 6.   TAP TEST

6.1   Impact Test Panel (A-20)

The computer aided tap tester was first applied to the A-20 impact panel. The data is collected using the supplied software with the CATT. The contact time and the stiffness are shown in Fig. 6.1. The damaged area in the center of each image is depicted as an area of longer contact time and lower stiffness. The tap duration or contact time are shown in microseconds and the stiffness in MegaNewton per meter.

a) Tap duration   b) Stiffness
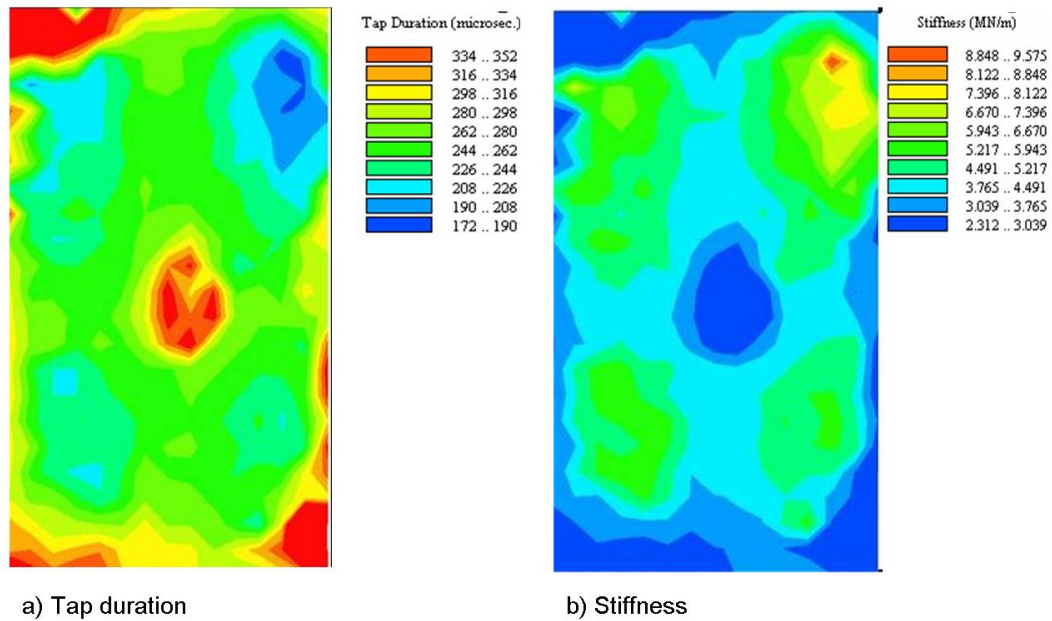
Figure 6.1   CATT images of the A-20 panel with a) tap duration and b) stiffness.

6.2 Carbon Spar Areas

The computer aided tap test was utilized to test the entire web section of both carbon wing spar sections. The tests were performed with a hand probe on the tool side of the web. A grid was laid out on the web and each cell was tapped by hand with the CATT. Figure 6.2 shows the contact time image produced on CS1. From the tap test image of CS1 it is difficult to identify the impact damaged regions. There is a noticeable difference in the uniformity of the thin web of the spar. This nonuniformity is a product of the thickness change and damage caused by the previous joint pull-off testing done by Cirrus prior to CNDE receiving the spar sample. The impact damage locations, shown in Fig. 6.3, are marked by circular borders in the image produced from CS2. All impact damages are visible in CS2 except for the two impacts near the ends of the spar. It is probable that the damages are masked in part by the edge effects associated with the end of the spar. Tap tests were performed on the caps of CS1 but no useful data was produced. The caps may have been virtually undamaged by the impacts in the cap region. Even though the tap tester is designed to work on thin face sheets of a composite honeycomb core structure, it did prove effective in both the thick and thin web region.
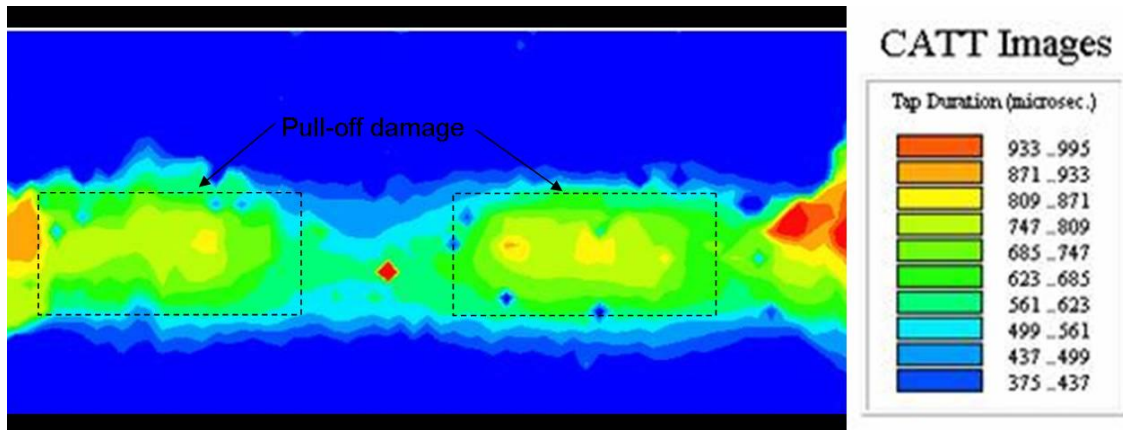
Figure 6.2   The image produced from the web of CS1 depicting tap duration.
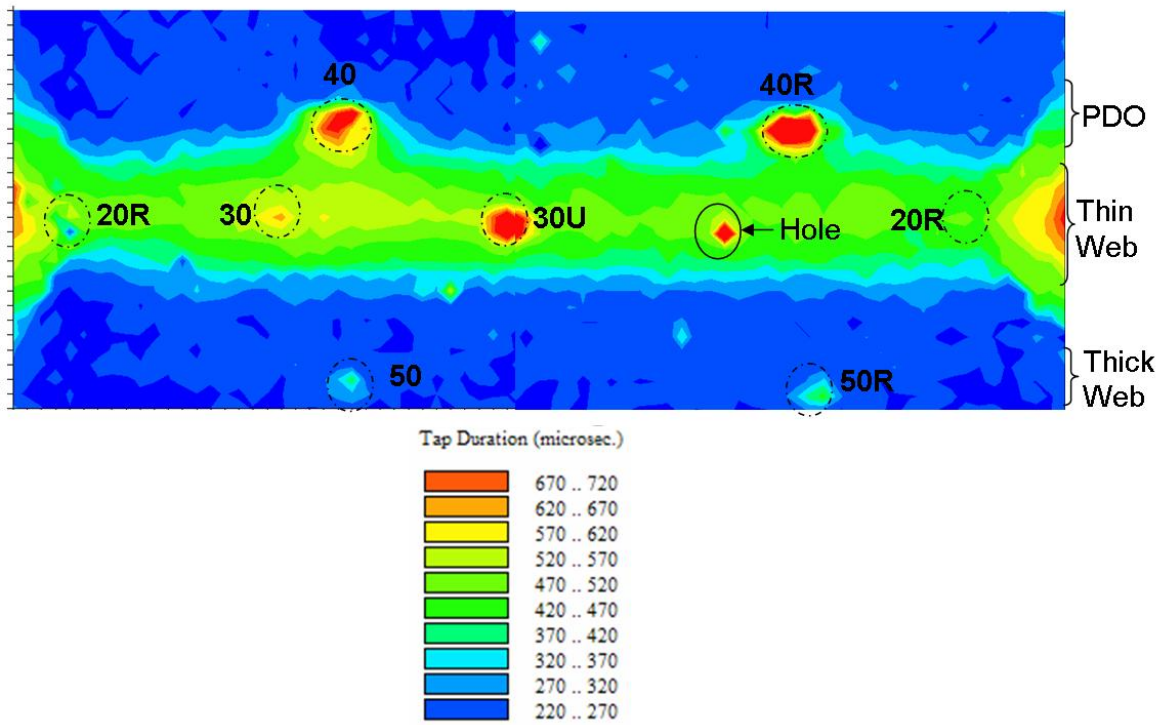
Figure 6.3   The image produced from the web of CS2 depicting tap duration.

CHAPTER 7.   PITCH-CATCH ULTRASOUND

7.1   Impact Damaged Panel

The pitch-catch system was first demonstrated by finding impact damage in a woven glass fiber laminate. The 24-ply laminate had been impacted by 16.6 Joules of energy with a 0.5" diameter impactor. The initial amplitude C-scan of this damage was created with the long dimension of the transducer holder along the horizontal axis of the scan and can be seen in Fig. 7.1. The Rayleigh wave transducers in the holder with a nose-to-nose configuration have a rectangular footprint. The unsymmetrical shape of this configuration will distort the appearance of a damaged region in the amplitude C-scan image. The distortion is dependent on the orientation of the transducer and the elongation effects are seen in Fig. 7.2. The orientation of the transducers is measured from the horizontal axis of the scan. Black represents the lowest signal amplitude while white represents the highest amplitude.
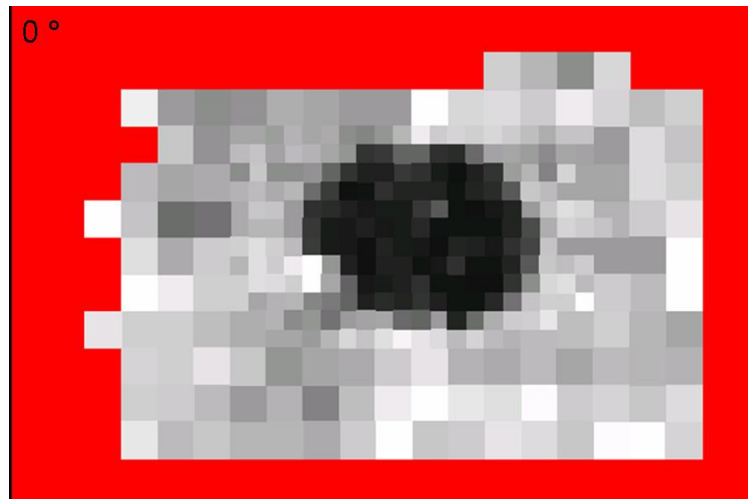
Figure 7.1   Pitch-catch amplitude C-scan image produced with Epoch 4 and GenScan with transducer at 0 degrees.
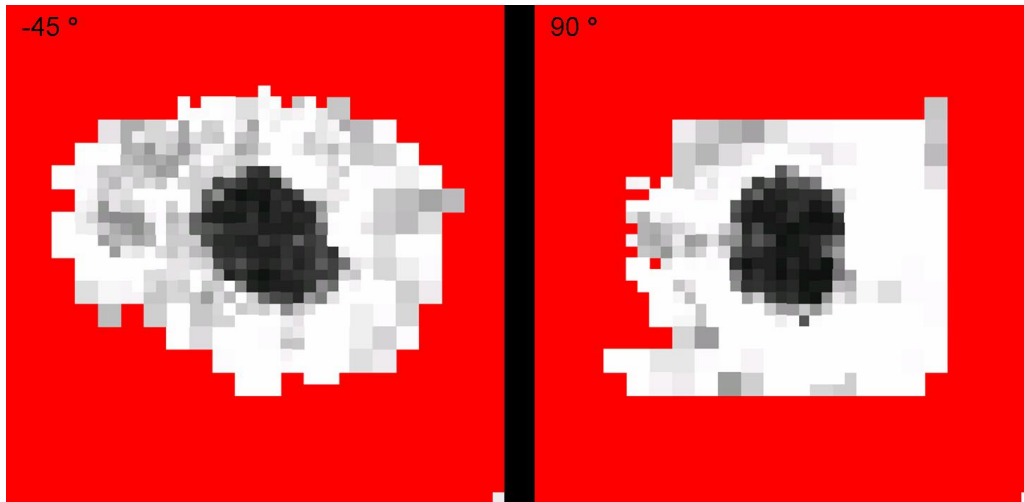
Figure 7.2   Amplitude C-scan images produced with Epoch 4 and GenScan
of 16.6 Joule impact area in the 24-ply woven glass panel with
transducers at -45 and 90 degrees.

7.2   Tedlar, Brass, and Nylon Embedded Object Panel (TBN)

The TBN embedded object panel was next to be investigated with the pitch-catch system. This panel had a series of square inserts of three different materials placed in the CFRP unidirectional lay-up during construction. The Tedlar, Brass, and Nylon inserts were placed in pairs, with a 1/2" and a 1/4" insert of each material placed next to each other in the same layer during manufacture of the panel. This panel was originally used to explore the effects of varying depths of defects on air-UT. The pitch-catch system demonstrates its capability to detect embedded objects in Fig. 7.3.
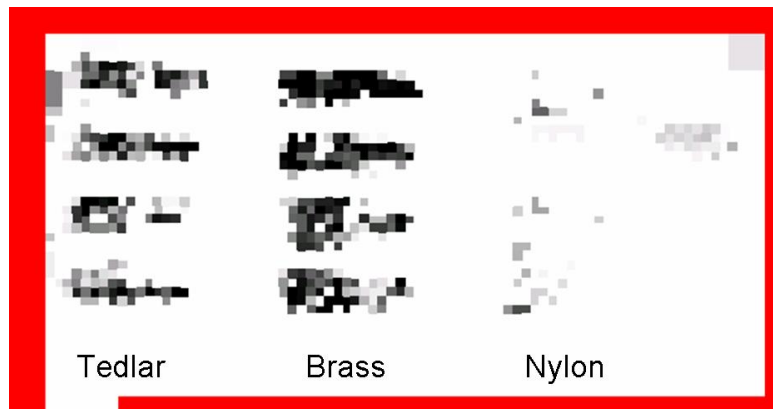
Figure 7.3   Amplitude C-scan image produced with the pitch-catch system
of the embedded object panel.

7.3 Carbon Spar

Amplitude C-scans using the pitch-catch method were made on the CS1 carbon spar. Figure 7.4 shows the 20 Joule impact damage area in the thin web of the CS1 spar. This was made using the Rayleigh wave, 2.25 MHz, transducers with the Epoch 4 flaw detector. The transducers were orientated at -45 degrees. The image produced with the same setup of the 30 Joule impact site can be seen in Fig. 7.5. Amplitude C-scans of the supported and unsupported impact sites on the cap of the carbon spar as well as the 10 Joule impact damage in the thin web were undistinguishable in the pitch-catch C-scan images.
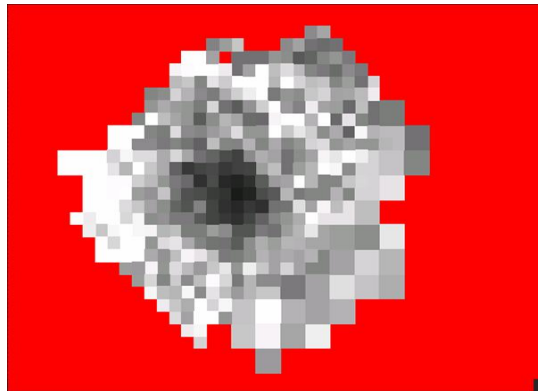
Figure 7.4   Amplitude image produced with Epoch 4 and GenScan of 20 Joule impact area in web of CS1.
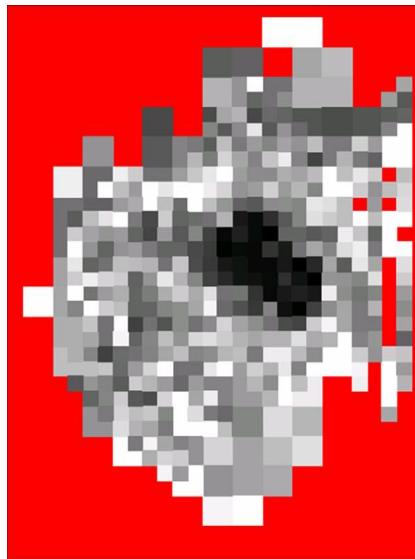
Figure 7.5   Amplitude image produced with Epoch 4 and GenScan of 30 Joule impact area in web of CS1.

CHAPTER 8.   CONCLUSION

Air-coupled ultrasonic tests conducted on the Cirrus carbon spar sections showed that impact damages induced at various locations on the spar within the energy range of concern to Cirrus were detectable with air-UT C-scan imaging equipment. At the low frequencies that are commonly used in air-UT, and given the complex morphology of the impact damage, the through transmitted ultrasonic amplitude in air-UT often exhibits unusual resonance, diffraction, and interference effects. As a result, the flaws or damages may appear in the C-scan image as a decrease or an increase of the transmitted amplitude. Although an increase in amplitude is counterintuitive from an energy blockage point of view, both types of features would signal an anomaly in the otherwise uniform structure. Most of the scan images presented in this thesis were generated using a mechanized scanner in the laboratory, but a manual, portable scanner, the GenScan, was also used in this research.

In addition to the main thrust of applying air-coupled ultrasonic imaging to the Cirrus spar, some material characterization experiments were also done. Additional techniques developed previously at CNDE, namely the Computer Aided Tap Tester (CATT) and the pitch-catch angle beam ultrasonic technique, were utilized to aid in the inspection of the carbon spar. These techniques are viewed to be useful for localized mapping of the flaws to gain further details after they are revealed in a quick survey with air-UT.

The image processing method presented utilizes an open-source image processing software with a simple internal script language that allows the user to automate the processing of hundreds of images. The percent porosity results from the image processing method correlate well with the acid digestion results for woven and quasi-isotropic laminates. The image processing method only inspects one plane in a lay up and with the varying morphology of porosity the percent porosity can vary greatly from one plane to the next, especially in unidirectional laminates. It therefore may be necessary to analyze more than one plane if the material property is highly nonuniform. The method described is a viable method for determining the porosity content in both glass and carbon reinforced composites.

APPENDIX.   IMAGE TOOL SCRIPT

```
macro 'Autoporosity';                                  'Comments
    var                                                'Declare variables
    thresh : integer;
    filt : string;
    winname : string;
    counter : integer;
begin                                                  'Beginning of program
    For counter:=301 To 450 Do Begin                   'Begin Do Loop
                                                       'Label all images por1,
                                                        por2,etc
                                                       'The number is the
                                                        counter variable
    Open('C:\\Storage location\\por',counter,'.jpg'); 'Allows opening
                                                        of proper image


    plugin('makegray');                                'Color to grayscale
                                                        command

    updatewindow;                                      'Updates image in open
                                                        window

    choosepic(1,1);                                    'Selects image
    ChangeValues(120,255,255);                         'Upper threshold value
    changevalues(0,119,0);                             'Lower threshold value
    UpdateWindow;
    Filter('smooth more');                             'Filter command
    updatewindow;                                      'Repeat until only
    ChangeValues(100,255,255);                          porosity is left
    changevalues(0,99,0);
    UpdateWindow;
    Filter('smooth more');
```

```
    updatewindow;
    ChangeValues(175,255,255);
    changevalues(0,174,0);
    UpdateWindow;
    plugin('bwcount');                          'Counts black and white
                                                 pixels to get area of
                                                 porosity data

    closeall;                                   'Close all windows
    end;                                        'End of Do Loop
end;
```

BIBLIOGRAPHY

[1] Cirrus Design Corporation, 4515 Taylor Circle, Duluth, MN 55811

[2] Center for Nondestructive Evaluation, 1915 Scholl Road, Ames, IA 50010

[3] Advanced Structural Imaging Inc., 2014 North Dakota Avenue, Ames, IA 50014

[4] The Ultran Group, 3100 Research Drive, State College, PA 16801

[5] Quality Material Inspection Inc., 5442 Oceanus Drive, Huntington Beach, CA 92649

[6] D.J. Barnard, J.J. Peters, D.K. Hsu, "Towards a Generic Manual Scanner for Nondestructive Inspection", Rev. of Prog. in Quantitative NDE, Vol. 24, edited by D.O. Thompson and D. E. Chimenti, AIP, Melville, New York, 2005. pp. 1669-1676

[7] I. M. Daniel, S. C. Wooh, and I. Komsky,"Quantitative Porosity Characterization of composite materials by means of ultrasonic attenuation measurements," Journal of Nondestructive Evaluation, Vol. 11-1, Springer Netherlands, 1992. pp. 1-8

[8] D. K. Hsu and K. M. Uhl, "A Morphological Study of Porosity Defects in Carbon-Epoxy Composites," Review of Progress in Quantitative NDE, Vol. 6B, edited by D. O. Thompson and D. E. Chimenti, AIP, Melville, New York, 1987. pp. 1019-1026

[9] D. K. Hsu and S. M. Nair, "Evaluation of Porosity in Graphite Epoxy Composites by Frequency Dependence of Ultrasonic Attenuation," Review of Progress in Quantitative NDE, Vol. 6B, edited by D. O. Thompson and D. E. Chimenti, AIP, Melville, New York, 1987. pp. 1185-1193

[10] M. P. Connolly, "The Measurement of Porosity in Composite Materials Using Infrared Thermography," Journal of Reinforced Plastics and Composites, Vol. 11, No. 12, Sage Publications, 1992. pp. 1367-1375

[11] ASTM D 3171-2006, "Standard Test Method for Constituent Content of Composite Materials."

[12] The University of Texas Health Science Center in San Antonio

[13] SONIX Corporation, 8700 Morrissette Drive, Springfield, VA 22152

[14] Olympus NDT Inc., 48 Woerd Avenue, Waltham, MA 02453

[15] J. Peters, V. Kommareddy, Z. Liu, D. Hsu, "Non-Contact Inspection of Composites Using Air-Coupled Ultrasound", Rev. of Prog. in Quantitative NDE, Vol. 22, edited by D.O. Thompson and D. E. Chimenti, AIP, Melville, New York, 2004. pp. 973-980

[16] V. Kommareddy, J.J. Peters, V. Dayal, D.K. Hsu, "Air-Coupled Ultrasonic Measurements in Composites", Rev. of Prog. in Quantitative NDE, Vol. 23, edited by D.O. Thompson and D. E. Chimenti, AIP, Melville, New York, 2004. pp. 859-866

[17] D.K. Hsu, D.J. Barnard, J.J. Peters, V. Dayal, "Physical Basis of Tap Test as a Quantitative Imaging Tool for Composite Structures on Aircraft", Rev. of Prog. in Quantitative NDE, Vol. 20, edited by D.O. Thompson and D. E. Chimenti, AIP, Melville, New York, 200. pp. 1857-1864

[18] D.W. Schindel, D.A. Hutchins, W.A. Grandia, Ultrasonics, 34,(1996), 621

[19] D.K. Hsu, Preliminary Summary of Air-Coupled Ultrasonic Inspection of Cirrus Main Spar, 2005